Uncertainties in the effects of organic aerosol coatings on polycyclic aromatic hydrocarbon concentrations and their estimated health effects

Sijia Lou[1,2,3], Manish Shrivastava[4], Alexandre Albinet[5], Sophie Tomaz[5,6], Deepchandra Srivastava[5,7], Olivier Favez[5], Huizhong Shen[8], Aijun Ding[1,2,3]

[1]Joint International Research Laboratory of Atmospheric and Earth System Sciences, School of Atmospheric Sciences, Jiangsu Provincial Collaborative Innovation Center of Climate Change, Nanjing University, Nanjing, 210023, China

[2]Frontiers Science Center for Critical Earth Material Cycling, Nanjing University, Nanjing 210023, China

[3]State Key Laboratory of Severe Weather Meteorological Science and Technology, Nanjing University, Nanjing 210023, China

[4]Pacific Northwest National Laboratory, Richland, WA 99354, USA

[5]Institut National de l'Environnement industriel et des RISques (INERIS), 60550, Verneuil en Halatte, France

[6]now at: INRS, 1 rue du Morvan CS 60027, 54519, Vandoeuvre-lès-Nancy, France

[7]now at: School of Geography Earth and Environmental Science, University of Birmingham, Edgbaston, Birmingham, UK B15 2TT

[8]Shenzhen Key Laboratory of Precision Measurement and Early Warning Technology for Urban Environmental Health Risks, School of Environmental Science and Engineering, Southern University of Science and Technology, Shenzhen 518055, China

Correspondence to: Sijia Lou (lousijia@nju.edu.com); Manish Shrivastava (ManishKumar.Shrivastava@pnnl.gov)

Abstract.

We used the CAM5 model to examine how different particle-bound Polycyclic Aromatic Hydrocarbon (PAH) degradation approaches affect the spatial distribution of benzo(a)pyrene (BaP). Three approaches were evaluated: NOA (no effect of OA coatings state on BaP), Shielded (viscous OA coatings shield BaP from oxidation under cool and dry conditions), and ROI-T (viscous OA coatings slow BaP oxidation in response to temperature and humidity). Results show that BaP concentrations vary seasonally, influenced by emissions, deposition, transport, and degradation approach, all of which are influenced by meteorological conditions. All simulations predict higher population-weighted global average (PWGA) fresh BaP concentrations during December-January-February (DJF) compared to June-July-August (JJA), due to increased emissions from household activities, and reduced removal processes during colder months. The Shielded and ROI-T approaches, which account for OA coatings, result in two to six times higher BaP concentrations in DJF compared to NOA. The Shielded simulation predicts the highest PWGA fresh BaP concentration (1.3 ng m^{-3}), with 90% of BaP protected from oxidation. In contrast, the ROI-T approach forecasts lower concentrations in mid-to-low latitudes, as it assumes less effective OA coatings under warmer, more humid conditions. Evaluations against observed BaP concentrations show the Shielded approach performs best, with a normalized mean bias (NMB) within ±20%. The combined incremental lifetime Cancer risk (ILCR) for both fresh and oxidized PAHs is similar across simulations, emphasizing the importance of considering both forms in health risk assessments. This study highlights the critical role of accurate degradation approaches in PAH modelling.

1 Introduction

Polycyclic aromatic hydrocarbons (PAHs), emitted from incomplete combustion of biofuels and fossil fuels, are persistent organic pollutants composed of multiple aromatic rings. Some of them are contaminants of global concern due to their well-known carcinogenic and mutagenic properties, which increase the risk to human health [Boffetta et al., 1997; Perera, 1997; Chen and Liao, 2006; IARC, 2010; Kim et al., 2013; Muir et al., 2019]. For instance, in 1976, the United States Environmental Protection Agency (US EPA) listed 16 PAHs as priority pollutants [Keith 2015]. Among these, particle-bound PAHs are more carcinogenic than gas-phase PAHs [Y Liu et al., 2017]. Therefore, benzo(a)pyrene, one of the most carcinogenic PAHs and predominantly existing in the particle phase, is often used as an indicator of cancer risk resulting from exposure to PAH mixtures [EPA 2004; EPCEU 2004; MEPPRC 2009; CPCB, 2020; IARC, 2021]. Considering that lifetime exposure to 0.1 ng m^{-3} of BaP would increase the additional lung cancer risk by one in 100,000 exposed persons, the World Health Organization (WHO) recommends limiting BaP concentrations to 0.1 ng m^{-3} [WHO, 2000; Bostrom et al., 2002].

High levels of BaP in ambient air have been measured globally over the past two decades, ranging from 0.1 to 2.5 ng m^{-3} in Europe and North America, with even higher concentrations observed in rural areas of China and India, exceeding 10 ng m^{-3} [Lee et al., 2011; W Wang et al., 2011; Kim et al., 2012; Brown et al., 2013; Hu et al., 2017; 2018; Radonić et al., 2017; Ma et al., 2018; J Han et al., 2019; Lhotka et al., 2019; Munyeza et al., 2019; Ahad et al., 2020; Kumar et al., 2020]. However, compared to measurements, previous regional or global models suffer from large uncertainties, with biases spanning several orders of magnitude, largely due to an incomplete understanding of the complex gas-particle partitioning [Friedman et al., 2014; Galarneau et al., 2014; Lammel et al., 2015; Shrivastava et al., 2017; Mu et al., 2018; F Han et al., 2022]. For example, Iakovides et al. (2021) reported that using an octanol-air partition coefficient absorption model, such as the Junge-Pankow model, the gas-particle fractions of simulated PAHs are more suitable for remote or rural areas but not for urban areas. To differentiate between aerosols in European urban or rural areas, Arp et al. (2008) developed polyparameter linear free energy relationships (ppLFER) equations. Shahpoury et al. (2016) reported that the ppLFER model can distinguish a variety of organics, including liquid water-soluble/organic soluble organics, and solid/semisolid organic polymers, as well as the inorganic phases of aerosols. Therefore, by adopting the ppLFER scheme, the gas-particle partitioning of simulated PAHs in anthropogenically impacted areas is improved, and the simulated PAHs show good agreement with observations [Tomaz et al., 2016; Kelly et al., 2021].

The lack of clarity regarding the chemical loss of PAHs is a significant factor contributing to large deviations in model-simulated BaP concentrations compared to measured values. As a semi-volatile compound, BaP in the gas-phase undergoes degradation through various pathways, primarily involving reactions with hydroxyl radicals (OH) and nitrate radicals (NO$_3$), along with photolytic processes driven by light. In a particle-bound state, while BaP can also be degraded by OH and NO$_3$, this occurs at a much slower rate compared to degradation by ozone, which serves as the primary mechanism in this phase [Keyte et al., 2013]. Laboratory studies have shown that particle-bound BaP can undergo rapid oxidation within hours through heterogeneous chemical degradation of BaP on the surface of black carbon (BC), organic carbon (OC), and sulfate aerosols [Pöschl et al., 2001; Kwamena et al., 2004; Kahan et al., 2006; Zhou et al., 2012]. Despite laboratory findings, field measurements have revealed that BaP persists in the atmosphere for extended periods and can be transported over long distances, reaching even the Arctic

[Halsall et al., 1997; Masclet et al., 2000; Schauer et al., 2003; Lohmann and Lammel, 2004; Van Overmeiren et al., 2024]. A recent laboratory study demonstrated that the presence of secondary organic aerosol (SOA) coatings could shield BaP from ozone oxidation [Zelenyuk et al., 2012]. Based on this, Friedman et al. (2014) used an exponential decay function, assuming that 80% of SOA-bound PAHs were still present after 24 hours. However, the shielding effectiveness of PAHs depends on the phase state of SOA, which should be temperature- and relative humidity-dependent [Koop et al., 2011; Zhou et al., 2013; Berkemeier et al., 2016; Shiraiwa et al., 2017; Shrivastava et al., 2017; Mu et al., 2018]. Shrivastava et al. (2017) developed a new PAH modeling approach in the global Community Atmosphere Model, assuming that viscous SOA can completely inhibit particle-bound PAHs (i.e., BaP) oxidation reactions under cool or dry conditions. Implementing this approach significantly improved the agreement between simulated and measured BaP concentrations at hundreds of locations worldwide compared to models that ignored the shielding effects of SOA coatings. Meanwhile, Mu et al. (2018) suggested that shutting off particle-bound BaP degradation based on the simple thresholds of temperature and relative humidity used in Shrivastava et al. (2017) cannot represent the complex multiphase reactions of BaP. They proposed a new ROI-T approach, accounting for the effects of temperature and humidity on SOA phase state and BaP degradation chemical reaction rate. The BaP concentrations simulated using the ROI-T approach exhibited the best agreement with measurements at Xianghe (China) and Gosan (South Korea) sites [Mu et al., 2018]. However, their simulations still showed a significant underestimation of BaP concentrations for European and Arctic background sites.

Although simulations of PAHs have significantly improved over the past decade [Sehili et al., 2007; Friedman & Selin, 2012; Shen et al., 2014; Shrivastava et al., 2017; Mu et al., 2018; Wu et al., 2024], particularly in terms of lifetime estimation, understanding of the oxidation chemistry remains a key area of development. The oxidation of particle-bound BaP is highly dependent on the concentrations of oxidants (primarily ozone) and the effectiveness of shielding by viscous organic aerosol (OA) coatings, which are influenced by temperature and relative humidity (RH). This dependence results in notable seasonal variations in both fresh BaP concentrations and oxidized BaP. Since assessments of PAH-induced lung cancer risks often rely on modeled BaP concentrations [Shen et al., 2014; Shrivastava et al., 2017; F Han et al., 2020; 2022; Famiyeh et al., 2021; Li et al., 2022; Wu et al., 2024], uncertainties in these simulations can have significant implications for estimates of PAH exposure and associated human health risks. This study systematically evaluates the uncertainty in simulated BaP concentrations due to varying chemical mechanisms of BaP oxidation, considering seasonal variations. This paper also assesses the strengths and limitations of current PAH modelling approaches, offering insights into future simulation improvements. The structure of the paper is organized as follows: Section 2 introduces the model, particle-bound BaP degradation approaches, emissions, and observation data used in this study. Section 3 first presents the simulated fresh and oxidized BaP concentrations in winter and summer, followed by a detailed comparison between simulated BaP and measurements, as well as an assessment of PAH-related lung cancer risk. Section 4 gives the conclusions and implications for discussions.

2 Methods

2.1 Measurements

We collected observed fresh BaP concentrations at 66 background/remote sites and 208 non-background sites worldwide (Table S1, S2). The observation data of fresh BaP were obtained from the Integrated Atmospheric Deposition Network (IADN, available from https://www.epa.gov/great-lakes-monitoring/great-lakes-integrated-atmospheric-deposition-network), the European Monitoring and Evaluation Programme (EMEP, available from https://www.emep.int [Tørseth et al., 2012]), the Global Environmental Assessment Information System (GENASIS, available from https://www.genasis.cz [Boruvkova et al., 2015]), the Arctic Monitoring and Assessment Programme (AMAP [Hung et al., 2010]), and previous studies [Shen et al., 2014; Shrivastava et al., 2017]. For oxidized BaP, measurements were available from only two locations: Grenoble—an urban site situated at 5.73°E, 45.16°N—in 2013, and SIRTA—a background site located at 2.15°E, 48.71°N (http://sirtaa.ipsl.fr/)—in the years 2014-2015. However, due to the measurement limitations, data on oxidized BaP (primarily nitro-BaP) were only available from two sites in France. Therefore, this study only includes concentrations of oxidized BaP from Grenoble (an urban site located at 5.73E, 45.16ºN) in 2013 [Tomaz et al., 2016] and from the ACTRIS SIRTA atmospheric supersite (Site Instrumental de Recherche par Télédétection Atmosphérique, which is representative of the suburban background site in the Paris region, located at 2.15°E, 48.71°N; http://sirtaa.ipsl.fr/) in 2014-2015 [Lanzafame et al., 2021]. The Grenoble site is centrally located and represents a location with significant urban influence, while the SIRTA site is located 25 km southwest of central Paris and is considered representative of regional background air quality.

2.2 Overview of the model

We employed the global Community Atmosphere Model version 5.2 (CAM5) to simulate the global distribution of BaP concentrations. Tracer concentrations obtained from CAM5 simulations were performed at a horizontal resolution of 1.9 ° latitude by 2.5 ° longitude, and a vertical resolution of 30 layers between the surface and 3.6 hPa. The Model for Ozone and Related Chemical Tracers (MOZART-4) represented the gas-phase chemical mechanism [Emmons et al., 2010], while the properties and processes of aerosol species were included in the Modal Aerosol Model (MAM3) [X Liu et al., 2012]. The model encompassed six aerosol species, including inorganic aerosols (e.g. mineral dust, black carbon, sulfate, and sea salt) and organic aerosols (primary organic aerosol and secondary organic aerosol). In addition, this study utilized an update of the volatility basis-set (VBS) approach developed by Shrivastava et al. (2015). The VBS approach tracked SOA formation based on SOA precursor gas sources, addressing both functionalization and fragmentation reactions during multi-generational aging of SOA precursor gases, as well as oligomerization reactions of SOA. The ppLFER (polyparameter linear free energy relationships) model was applied to the gas-particle partitioning of BaP, encompassing both BaP absorption into organic aerosols and adsorption onto the surface of black carbon aerosol [Shahpoury et al., 2016]. Following Shrivastava et al. (2017), we divided OA into the liquid water-soluble/organic soluble phase and the solid/semi-solid organic polymer phase. More than 90% of particle-bound BaP is absorbed within organic aerosols after applying the ppLFER model. The transport, dry deposition, and

179 wet removal of particle-bound BaP (including oxidized PAH) are treated similarly to other aerosol
180 species in CAM5 [X Liu et al., 2012].
181   The viscosity of OA affects the atmospheric lifecycle of BaP in two ways: (1) through the gas-particle
182 partitioning of SOA, which also impacts the gas-particle partitioning of BaP (as described by the pp-
183 LFER approach), and (2) by altering the heterogeneous degradation kinetics of BaP with ozone. In the
184 following section, we describe the application of three different model sensitivity formulations that
185 account for the role of OA viscosity on the lifecycle of BaP.

186 **2.3 BaP degradation**

187 The model incorporates the gas-phase reaction of BaP with OH. Consistent with previous studies, the
188 second-order rate coefficient for the reaction of gaseous BaP with OH is set at 5×10^{-11} cm^3 molecules^{-1}
189 s^{-1} [Keyte et al., 2013; Shrivastava et al., 2017]. Heterogeneous reactions of particulate-phase BaP with
190 OH and ozone are also included in the model [Cazaunau et al., 2010; Zhou et al., 2012; 2013; Keyte et
191 al., 2013]. The second-order rate coefficient for the reaction of particle-bound BaP with OH is determined
192 to be 2.9×10^{-13} cm^3 molecules^{-1} s^{-1} [Esteve et al., 2006], which is two orders of magnitude slower than
193 the gas-phase reaction rate of BaP with OH. Conversely, particle-bound BaP reacts rapidly with ozone
194 within a few hours, representing the primary oxidation pathway for BaP. Note that the photolysis of BaP
195 is not included in this study, partly because its photolysis rate constant is much lower compared to that
196 of low molecular wight PAHs [Niu et al., 2007], and the current model already underestimates BaP
197 concentrations.
198 In this study, three approaches are implemented to estimate particle-bound BaP degradation, providing
199 insights into the uncertainty associated with this process.
200 (1) In the default NOA approach, the characteristics of the organic coating - such as its thickness and
201   viscosity - do not affect the heterogeneous loss of particle-bound BaP. In this approach, the oxidation
202   of BaP follows the Langmuir-Hinselwood mechanism, meaning that the reaction rate (k) is first-
203   order with respect to BaP and depends on ozone concentration. Since the reference state of the
204   organic coating in this approach is thin and liquid-like, diffusion limitations are not considered
205   significant [Zhou et al., 2012; 2013]. In addition, this approach does not consider the effects of OA
206   viscosity on the gas-particle partitioning of SOA, as it uses the FragSVSOA treatment described in
207   Shrivastava et al. (2015), which assumes SOA as semi-volatile liquid-like well-mixed solution
208   throughout its atmospheric lifetime.
209 (2) Following Shrivastava et al. (2017), the SOA Shielded approach is implemented, accounting for the
210   shielding of BaP by viscous SOA coatings. The kinetics of the heterogeneous oxidation of BaP with
211   ozone become much slower after absorption by organic aerosols, as thick OA coatings reduce the
212   kinetics of mass transfer of BaP from the interior of the particle to the particle surface. The
213   effectiveness of SOA shielding is related to its thickness and viscosity, influenced by temperature
214   and relative humidity [Zhou et al., 2012; 2013]. In this approach, when SOA coatings are less than
215   20 nm, we assume that SOA cannot effectively shield particle-bound BaP, and thus, the
216   heterogeneous oxidation kinetics remain the same as in the default NOA approach. Thick SOA
217   coatings (> 20 nm) can completely turn off the particle-bound BaP heterogeneous loss kinetics under
218   dry or cool conditions (RH < 50% or temperature < 296 K). Different oxidation kinetics with ozone
219   are applied under humid (RH $\geq$ 50%) and warm (temperature $\geq$ 296 K) conditions with thick SOA

220   coatings, where the second-order rate coefficient for the reaction of particle-bound BaP with ozone

221   is 14 and 6.2×10^{-15} cm^3 molecules^{-1} s^{-1} under moderate humidity ($50\% \leq RH < 70\%$) and high

222   humidity conditions ($RH \geq 70\%$), respectively [Zhou et al., 2013; Shrivastava et al., 2017].

223 (3) Following Mu et al. (2018), the ROI-T approach is implemented, accounting for the temperature

224   and humidity dependence of the phase state, diffusivity, and reactivity of particulate-phase BaP.

225   First-order reaction rate coefficients for BaP ozonolysis are sensitive to both temperature and RH

226   below room temperature (296 K), but are only temperature sensitive above room temperature [Mu

227   et al., 2018] (Table S1). Under cool and dry conditions, the first-order reaction rate coefficients are

228   3-4 orders of magnitude lower than those under warm conditions (Table S1). Notably, the ROI-T

229   approach yields a much slower oxidation reaction of particle-bound BaP than the default NOA

230   approach under cool and dry conditions but a faster oxidation reaction rate under warm conditions.

231 Note that both the Shielded and ROI-T approaches described above consider the impact of aged semi-

232 solid SOA on the gas-particle partitioning of fresh SOA precursors, using the FragNVSOA treatment

233 described in Shrivastava et al. (2015). This treatment assumes that, once SOA is formed, it is transformed

234 into a highly viscous, non-volatile semi-solid within the same global model timestep (30 min) due to

235 particle-phase oligomerization reactions within the SOA [Shrivastava et al., 2015]. The FragNVSOA

236 treatment also assumes that any further gas-phase organic oxidation products that condense do not form

237 a solution with pre-existing OA. This assumption is supported by recent experimental studies, which

238 show a short aging timescale of ~20 min, during which oligomer and organosulfate formation within

239 isoprene SOA, leading to non-equilibrium partitioning behaviour and phase transition to semi-solid SOA

240 [Chen et al. 2023].

241 **2.4 Model Sensitivity Simulations**

242 We conduct simulations using CAM5 to explore the uncertainty of seasonal variations in BaP

243 concentrations with different PAH oxidation approaches. Three effects of OA coatings on particle-bound

244 PAH oxidation, as detailed in section 2.3, are considered. Hence, sensitivity simulations are performed

245 as follows:

246   (1) NOA;

247   (2) Shielded [Shrivastava et al., 2017];

248   (3) ROI-T [Mu et al., 2018].

249 All simulations are conducted over two years (2007-2008), with the first year allocated for spin-up. Since

250 most observations occurred around 2004-2009, winds and temperature are nudged toward ERA-Interim

251 data from January 2007 to December 2008 in this study.

252 **2.5 Emissions**

253 This study utilizes the Global Emission Modeling System (GEMS) 0.1º × 0.1º global BaP emission

254 inventory with temporal and spatial variations, which is available from gems.sustech.edu.cn. The

255 inventory was derived from the PKU-PAH Global Emission Inventory [Shen et al., 2013], which

256 incorporates data from all major fuel consumption sources and industrial processes. The spatiotemporal

257 changes in global BaP emissions are detailed in our previous work [Shrivastava et al., 2017; Lou et al.,

258 2023]. Anthropogenic emissions, including BC, OC, and precursor gases for both secondary aerosols

259 and ozone, are sourced from the HTAP_v2.2 2008 emission inventory [Janssens-Maenhout et al., 2015].

260   Additionally, emissions from agricultural waste burning and open biomass burning emissions are
261   obtained from the Emissions Database for Global Atmospheric Research (EDGAR v4.3) and Global Fire
262   Emissions Database (GFED3.0), respectively [van der Werf et al., 2010; Crippa et al., 2018]. To maintain
263   consistency with the modeling timeframe and facilitate comparison with observations, all emissions are
264   set at 2008 levels.

2.6 Global model downscaling formulation

To enhance the comparison between simulated BaP concentrations and observational data, particularly
in anthropogenically influenced areas such as urban regions, we implemented a downscaling approach
based on a Gaussian diffusion algorithm. This method refined the model-derived near-surface BaP
concentrations from the coarse resolution of 2.5°×1.9° to a finer resolution of 0.1°×0.1°, aligning with
the original resolution of emission inventory. Following the methodology outlined by Shen et al. (2014),
we assigned a weighting factor (W_i) to each 0.1°×0.1° receiving grid cell. This factor was determined by
summing the contributions of emissions from all 0.1°×0.1° emission grid cells within a defined
neighbourhood. The neighbourhood consists of the 2.5°×1.9° model grid cell containing the receiving
grid cell and the eight adjacent model grid cells, encompassing approximately 4275 0.1°×0.1° emission
grid cells. The formulation for W_i is as follows:

$$W_i = \sum_{j=1}^{n} \frac{2.03 Q_j f_j e^{-r_d t_{ji}}}{u_j \sigma z_j x_{ji}} \qquad (1)$$

Here, Q_j (ng/s) represents the emissions density of the jth emission grid cell. f_j (dimensionless) and
u_j (m/s) are wind frequency (0-1) and wind speed in directions 1 to 16 (N, NNE, NE, NEE, E, SEE, SE,
SSE, S, SSW, SW, NWW, NW, and NNW) in the jth grid cell, respectively, taken from the ERA-interim
reanalysis wind field. The degradation rate r_d (/s) involves the gas-phase reaction with OH and the
particle-phase heterogeneous reaction with ozone in the receiving grid cell derived from the chemical
transport model. n represents the number of emission grid cells within the nine model grid cells and is
approximately 4275, though the actual value depends on the alignment of the grid resolutions.
Additionally, t_{ji} (s) and x_{ji} (m) denote the distance and transport time from the jth emission grid cell
to the ith receiving grid cell, and σ (m) is the vertical standard deviation of the concentrations. Finally,
the calculated W_i is used as a proxy to disaggregate the model-calculated concentration of each 2.5°×1.9°
model grid cell to a 0.1°×0.1° grid cell. Previous studies have reported substantial improvements in the
distribution and magnitude of observed BaP concentrations through this downscaling process in similar
simulations [Shen et al., 2014; Shrivastava et al., 2017; Lou et al., 2023].

2.7 Incremental Lifetime Cancer Risk

The Incremental Lifetime Cancer Risk (ILCR) induced by exposure to PAHs in ambient air is calculated
using the following formula [Shen et al., 2014]:

$$ILCR = CSF \times LADD \times SUS = CSF \times \frac{C \times IR \times y}{BW \times LE} \times SUS \quad (2)$$

where CSF, LADD, and SUS represent the cancer slope factor, lifetime average daily dose, and a factor
describing individual susceptibility, respectively. Following Shen et al. (2014), CSF of 26.6 kg (body
weight)·day/mg for BaP was adopted as the maximum likelihood estimate based on epidemiological data

298 from studies on coke oven workers, using a multistage type model [U.S. EPA, 1982]. SUS accounts for
299 individual variations in susceptibility and is defined as the product of genetic susceptibility (GeneSus),
300 ethnicity-adjusted factor (EAF), and age-sensitivity factor (ASF), respectively. GeneSus represents the
301 impact of genetic variations on an individual's susceptibility to BaP-induced cancer risk. Different
302 genotypes may lead to variations in metabolic activation or detoxification of PAHs, affecting
303 carcinogenic risk. EAF was calculated based on the lung cancer incidences for individual ethnicities
304 reported by the United States Cancer Statistics (available from https://www.cdc.gov/united-states-
305 cancer-statistics/index.html), excluding the effects of smoking. ASF accounts for age-related differences
306 in susceptibility to BaP exposure. Weighting cancer risk by a factor of 10, 2, and 1 were used for the age
307 groups of < 2, 2-16, and > 16 years, respectively [CA EPA, 2009].
308 LADD is calculated from BaP exposure concentration (C, mg m^{-3}), which is downscaled from model-
309 predicted BaP concentrations in this study, inhalation rate (IR, m^3/day), exposure duration (y, year), body
310 weight (BW), and average life expectancy of the global population (LE, 70 years). ILCR in this study is
311 a population-weighted average and represents the maximum likelihood estimate; the unit for ILCR is
312 one death per 100,000 persons.

313 **3 Results**

314 **3.1 Simulation of seasonal variations in global fresh BaP**

315 Given that lifetime exposure to 0.1 ng m^{-3} of BaP theoretically results in an additional lung cancer death
316 per 100,000 exposed persons, the WHO recommends a limit of 0.1 ng m^{-3} [Bostrom et al., 2002]. BaP
317 degradation approaches can significantly impact BaP concentrations, further influencing the assessment
318 of PAH exposure risks in various regions. Here, in this study, we investigated three different particle-
319 bound BaP degradation approaches related to the OA coating hypothesis to examine their effects on the
320 spatial distribution of BaP. Considering that the effectiveness of OA coatings is strongly dependent on
321 temperature and humidity variations, we analyzed the distribution of BaP concentrations under different
322 seasons.
323 In DJF (December-January-February), population-weighted global average (PWGA) BaP concentrations
324 with different particle-bound BaP degradation approaches are predicted to be 0.24-1.38 ng m^{-3},
325 consistently exceeding the WHO recommendation. High levels of BaP concentrations are simulated to
326 appear in East Asia, South Asia, North Africa, and Europe, with the peak BaP exposure in eastern China
327 exceeding 1.0 ng m^{-3} (Fig. 1). In contrast, BaP concentrations are much lower in JJA (June-July-August),
328 with PWGA values of 0.04-0.17 ng m^{-3}. These results indicate that the simulated BaP exhibits strong
329 seasonality, primarily influenced by changes in emissions, deposition, and BaP degradation chemistry.
330 Our simulated seasonal BaP concentrations, particularly for the ROI-T approach, align with a previous
331 study using the same emissions and particulate-BaP degradation approach [Wu et al., 2024].
332 In 2008, residential biomass use contributed more than 60% of total atmospheric BaP emissions for
333 households cooking, heating, and lighting [Shen et al., 2013]. Since the demand for heating and lighting
334 is higher in winter than in summer, more residential biomass burning is required in winter, inevitably
335 producing BaP. In addition, less precipitation in the Northern Hemisphere in winter compared to summer
336 (Fig. S1), linked to less efficient wet removal, contributes to the seasonal variations of BaP. Thus, without

337 the impacts of OA coatings on BaP degradation, the seasonal variations of BaP concentrations in
338 simulations using the NOA approach primarily represent the changes in emissions and deposition.

339
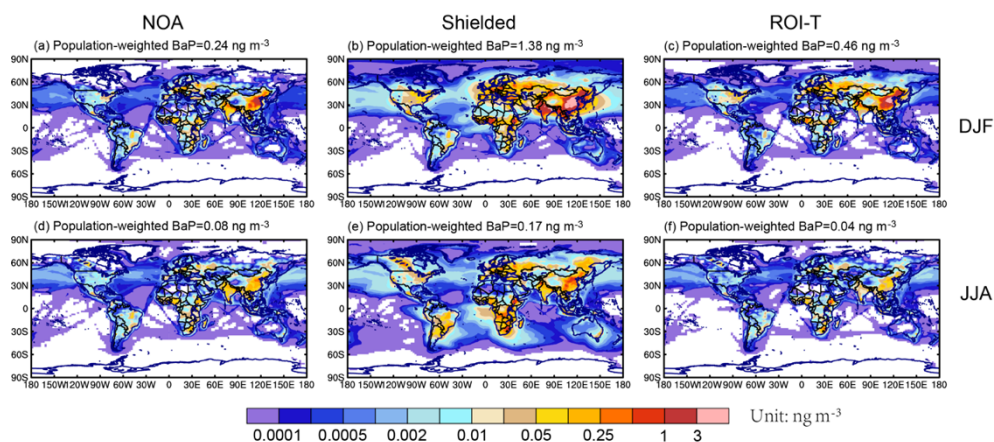
340 **Figure 1. The spatial distribution of simulated BaP concentrations in (a-c) DJF and (d-f) JJA. Fresh BaP**
341 **concentrations with different heterogeneous reaction approaches for particle-bound BaP are shown in the**
342 **left column (NOA), the middle column (Shielded), and the right column (ROI-T), respectively.**

343

344
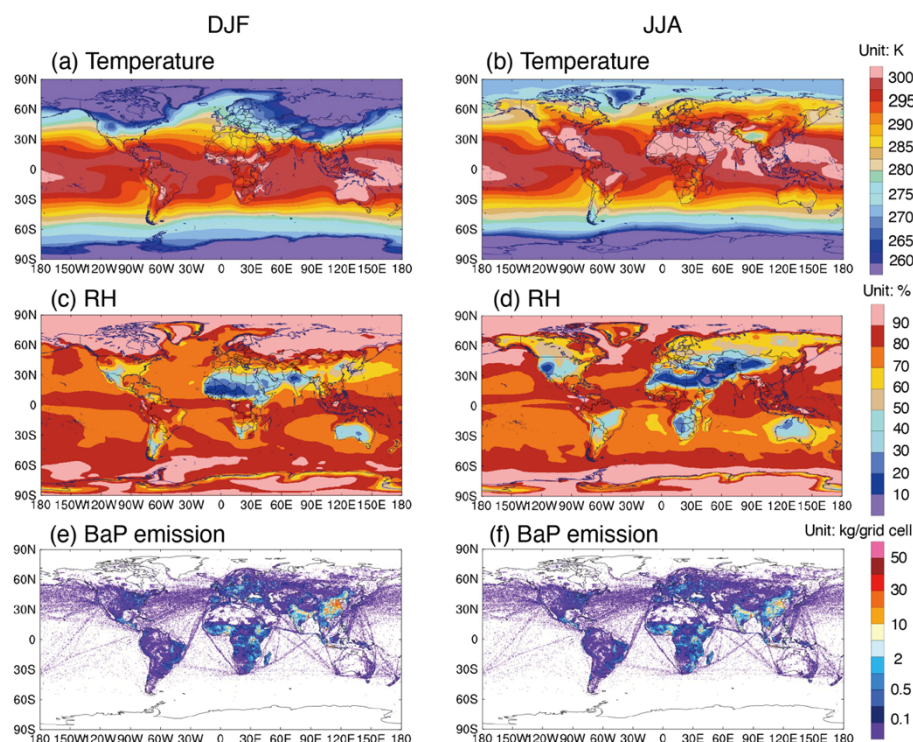
345 **Figure 2. The spatial distribution of surface-layer average temperature (top panel, unit: K), relative humidity**
346 **(middle panel, unit: %), and spatial distribution of BaP emissions (bottom panel, unit kg/grid cell) for both**
347 **DJF (December-January-February) and JJA (June-July-August) periods.**

348

349 Compared with simulations using the NOA approach, those incorporating OA coatings can effectively
350 impede the BaP loss process, leading to a significant increase in BaP concentrations during winter (Fig.
351 1). Upon absorption by organic aerosols, the presence of viscous OA coatings substantially hinders the

352 mass transfer kinetics of BaP from the particle core to the surface. The denser the organic aerosol, the
353 slower the diffusion of BaP, consequently slowing down the heterogeneous reactions of particle-bound
354 BaP with ozone and OH on the aerosol surface. This effect is more pronounced in winter than in summer,
355 attributed to cooler conditions that likely increase the viscosity of SOA [Shrivastava et al., 2017].
356 For example, the PWGA BaP from the simulation using the Shielded approach is six times higher than
357 that in the simulation using the NOA approach in DJF. With the Shielded approach, the OA coating is
358 assumed to be sufficiently tacky to prevent BaP from undergoing heterogeneous reactions with ozone
359 completely under dry or cool conditions, thereby extending the lifetime of BaP. During Northern
360 Hemisphere winters, effective OA shielding occurs in areas characterized by cool temperatures (<296 K)
361 or dry conditions (RH<50%), covering most of the regions with high BaP emission densities (Fig. 2a-b)
362 [Shiraiwa et al., 2011; Saukko et al., 2012; Zhou et al., 2012; Bateman et al., 2015]. Furthermore, BaP
363 with OA coatings can be transported over long distances to remote areas, including the Arctic. Treating
364 OA coating effectiveness as the ROI-T approach, the BaP concentrations also increase, with PWGA BaP
365 estimated to be twice as high as in the simulation with the NOA approach during winter. Compared with
366 the Shielded simulation, BaP concentrations in the ROI-T simulation exhibit similar spatial patterns in
367 high latitudes such as Europe, northern China, and the Arctic, but lower concentrations in southern China,
368 South Asia, and North Africa. The ROI-T approach assumes that the diffusion coefficients of BaP and
369 ozone within OA coatings decrease with reducing temperature and relative humidity, thus reducing the
370 degradation rate of BaP. That is, under cold (<273 K) or dry (<50%) conditions, such as mid-to-high
371 latitudes in winter (Fig. 2a, b), the degradation rates of BaP in the ROI-T approach are two to four orders
372 of magnitude smaller than those without the OA coating effect. In contrast, the OA coating in southern
373 China, South Asia and Africa is not as effective as those in Europe, northern China, and the Arctic,
374 resulting in BaP concentrations similar to NOA simulation.
375 In JJA, BaP concentrations tend to concentrate near the source areas. While BaP concentrations in the
376 simulation using the Shielded approach are estimated to be higher than those in the NOA simulation, the
377 concentrations found in the simulation using the ROI-T approach are even lower. The ROI-T approach
378 assumes that the diffusion coefficients of BaP and ozone increase with temperature, leading to an
379 estimated faster degradation rate of BaP than in NOA and Shielded approach simulations at conditions
380 above room temperature. Our results are consistent with previous studies [Shrivastava et al., 2017; Mu
381 et al., 2018].

3.2 Simulation of seasonal variations in global oxidized BaP

383 Previous modeling studies assumed that fresh PAHs are completely degraded after oxidation [Sehili and
384 Lammel, 2007; Matthias et al., 2009; Friedman et al., 2014]. However, laboratory experiments suggested
385 that several oxidized PAHs may remain particle-bound and even increase in molecular weight [Ringuet
386 et al., 2012; Zelenyuk et al., 2012; Jariyasopit et al., 2014]. Furthermore, not only fresh BaP but also
387 certain oxidized BaP species and derivatives exhibit toxicity [EHC 2003; Clergé et al., 2019; Hrdina et
388 al., 2022; Peng et al., 2023]. Therefore, it is essential to understand the impact of different BaP
389 degradation approaches on oxidized BaP.
390 In this study, we tracked oxidized particle-bound BaP, which is formed through the heterogeneous
391 reactions of particulate-phase BaP with OH and ozone. Figure 3 shows the spatial distribution of
392 simulated oxidized BaP concentrations in DJF. In the absence of an OA coating, particle-bound BaP is

always available to react with O_3. Therefore, most particle-bound BaP is rapidly oxidized near source areas, with a PWGA oxidized BaP concentration of 1.3 ng m^{-3}, or 82% of the total (sum of fresh and oxidized) BaP (Fig. 3a, d). If oxidized BaP is as toxic as fresh BaP, the oxidized BaP concentration in NOA globally exceeds the WHO recommendation of 0.1 ng m^{-3} by a wide margin. In comparison, the Shielded simulation predicts that high levels of oxidized BaP only appear in the tropics in winter (Fig. 3b), because OA coatings are less effective at protecting BaP from ozone attack under high temperature and high RH conditions (Fig. 2a, b). Since the viscous OA coatings completely shut down the particle-bound BaP oxidation reaction under cool or dry conditions, most fresh BaP can stay in the atmosphere for several days, with only 10% of the total BaP being oxidized. Surprisingly, although the OA coating slowed the diffusion of particle-bound BaP from inside the interior of the OA to the particle surface in the ROI-T simulation, 71% of the total BaP was still oxidized on a global basis.
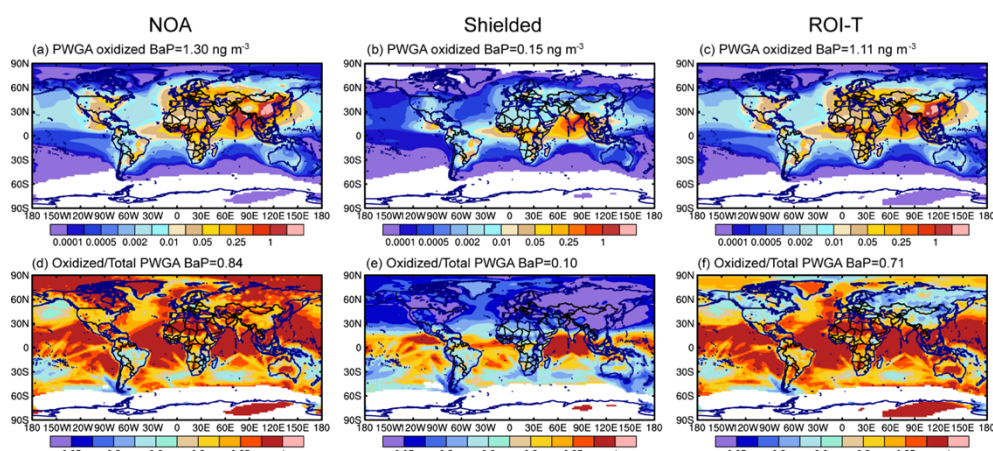
Figure 3. The spatial distribution of simulated (a-c) oxidized BaP concentrations and (d-f) the ratio of oxidized BaP to the total (fresh+oxidized) BaP in DJF. Simulations with the different heterogeneous reactions of particle-bound BaP approaches are shown in the left (NOA simulation), middle (Shielded), and right (ROI-T) columns, respectively.
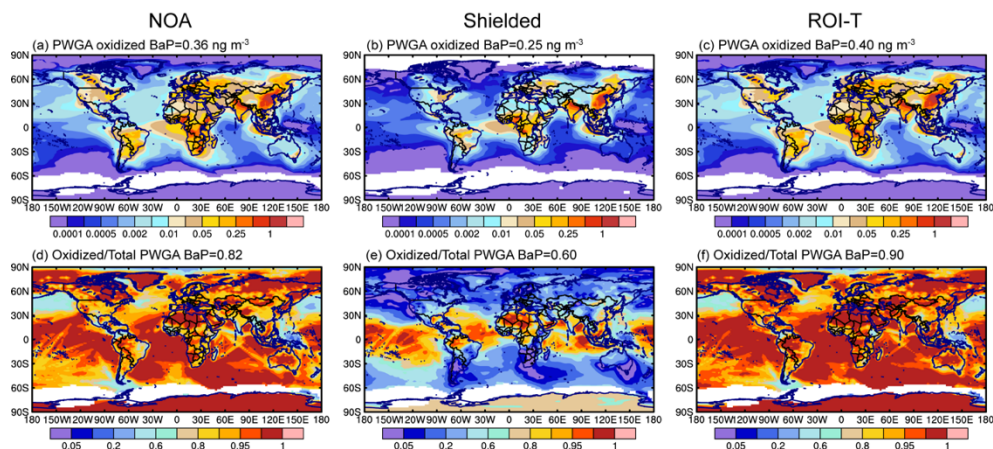
Figure 4. Same as Figure 3 but for JJA.

414   Due to the lower effectiveness of OA coatings under warm and moist conditions, all simulations with
415   different BaP degradation approaches predict that oxidized BaP contributes to more than 90% of the total
416   BaP concentrations in JJA in the tropics (30°S-30°N). At mid-to-high latitudes, the oxidized BaP varies
417   greatly with the effect of OA coatings on the BaP oxidation reactions. More than 80% of total BaP is
418   oxidized in mid-to-high latitudes applying the NOA or ROI-T approaches, with peaks exceeding WHO
419   recommendations in most of East Asia, West Europe, and North America. Meanwhile, the Shielded
420   approach assumes that OA coatings largely limit the particle-bound BaP oxidation reaction, whereas the
421   oxidized BaP contributes no more than 40% to the total BaP. Our results indicate that current model
422   estimates of human exposure to fresh or oxidized PAHs are highly sensitive to assumptions about PAH
423   degradation processing, especially during North Hemisphere winter.

424   **3.3. Model Evaluation**

425   **3.3.1 Fresh BaP**

426   To assess simulated BaP concentrations, we select surface BaP measurements from 66
427   background/remote sites and 208 urban-affected sites worldwide (Table S2, S3), covering the period
428   1997 to 2014, with a focus on the years between 2004 and 2011. Median BaP observations at each site
429   are compared with simulated BaP in DJF and JJA, respectively. Given the global model's horizontal grid
430   spacing of approximately 200 km, we specifically compare simulated BaP concentrations with
431   measurements from background sites. To address the limitations of the coarse global model, we
432   downscale the simulated BaP grid to a higher resolution of 10 km based on factors such as wind speed,
433   wind direction and frequency, emission density, and gas/particle BaP degradation rates to account for
434   strong gradients and high BaP concentrations near urban areas. This downscaled approach aims to
435   account for strong gradients and high BaP concentrations near source areas. Our previous studies, using
436   the same simulations, reported that while the coarse-grid model significantly underestimates
437   concentrations in urban-affected regions, the downscaled BaP vastly improves the comparison between
438   the model and observations [Shrivastava et al., 2017; Lou et al., 2023].
439   Figure 5a compares measured and model-predicted concentrations at 66 background sites around the
440   world in DJF. The model-estimated BaP for the Shielded approach during the same time and locations
441   of the measurements agrees best with observations of global BaP concentrations, with a normalized mean
442   bias (NMB) of -18%. In contrast, without the effect of OA coating on the degradation of particle-bound
443   BaP, NOA predictions are 78% lower than observed BaP globally (Fig. 5b). Comparisons between
444   measured and downscaled simulated BaP at urban-affected sites show similar results, as the OA shielding
445   approach significantly improves the model's ability to predict fresh BaP concentrations.
446   It's worth noting that the effectiveness of OA coatings depends largely on temperature and humidity,
447   which are related to the meteorological characteristics of different regions. We, therefore, compare
448   measured and model-simulated BaP concentrations at different latitudes, namely relatively high latitudes
449   (measured locations north of 40°N) and low latitudes (measured locations between 40°S and 40°N),
450   respectively. Figures 6a and 6b demonstrate that the OA shielding particle-bound BaP approach increases
451   the simulated BaP concentrations in much better agreement with the measured values than without the
452   OA coating effect. This improvement is not sensitive to latitude. For the ROI-T treatment, although
453   predicted fresh BaP concentrations at locations above 40°N were two or three times higher than the

454 treatment without OA coating effects, the simulation still substantially underestimates the BaP
455 concentrations in these regions by 50% (Fig. 6c). Moreover, model-estimated BaP concentrations in
456 ROI-T perform even worse at low latitudes compared to high latitudes. On a global average, the ROI-T
457 approach, accounting for the temperature and humidity dependence of the phase state, diffusivity, and
458 reactivity of particulate-bound BaP, underestimates BaP by ~60% in DJF (Fig. 5a, c).
459
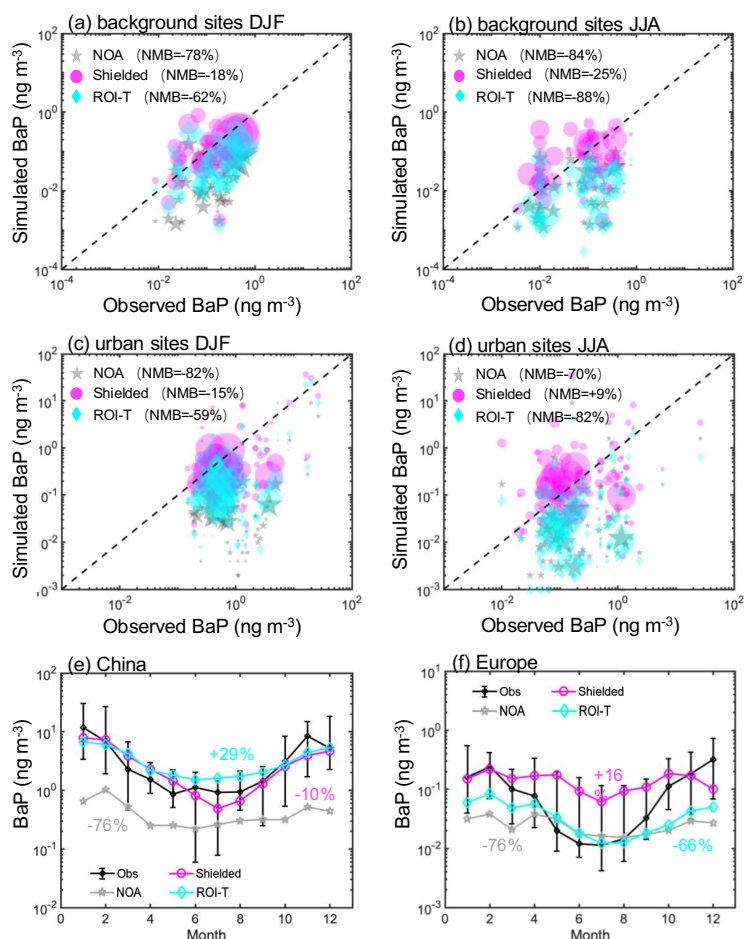
461 **Figure 5. Comparison between simulated surface BaP concentrations from NOA, Shielded, and ROI-T**
462 **simulations and ground-based measurements (a-b) for 66 background sites, (c-d) for 208 urban impacted sites.**
463 **The circle area is proportional to the number of days sampled at each site. Annual variation of measured and**
464 **simulated BaP concentrations at (e) 18 sites (6 background and 12 urban impacted sites) in China, and (f) 18**
465 **background sites in Europe. Black lines represent measured values (median and 15th and 85th percentiles of**
466 **site monthly means), while blue (NOA), red (Shielded), and green (ROI-T) lines represent the median of the**
467 **monthly model-simulated means for these sites.**

468

469 In JJA, both NOA and ROI-T simulations struggle to capture BaP concentrations, underestimating
470 observations by more than 70% (Fig. 5b and 5d). However, similar to DJF, the model-predicted
471 concentrations in simulation using the Shielded approach exhibit the best agreement with ground
472 measurements in JJA, showing a NMB of -25% and +9% at the background and urban-affected sites,
473 respectively. Interestingly, the ROI-T approach deviates more from the actual observed values, especially
474 at measurement locations between 40°N and 40°S (Fig. 6d and 6f).

475   Figure 5e indicates that both the Shielded simulation (red line) and ROI-T simulation (green line) capture

476   the magnitude and seasonal variations of BaP concentrations compared with monthly observations at 18

477   sites in China (black lines). The regions of China and Europe were chosen for this analysis because they

478   meet two criteria: (1) each has more than 10 measurement sites, and (2) the data from these sites span

479   over one year, allowing for a reliable representation of seasonal variations. In both simulations and

480   observations, BaP concentrations peak in winter but are lowest in summer. As mentioned in section 3.1,

481   the predicted monthly variations in BaP concentrations are due to the seasonality of BaP emissions and

482   BaP oxidation rates. For instance, residential emissions in China are four times higher in winter than in

483   summer, contributing 78% of BaP emissions in winter and 56% in summer [Shen et al., 2013].

484   Furthermore, lower wintertime temperatures favor more viscous OA coatings to reduce BaP diffusion

485   and decrease oxidation rates, while more liquid-like OA coatings in summer have a minor effect on BaP

486   oxidation reactions. In contrast, although the models show a similar seasonal cycle to observations, fresh

487   BaP concentrations are largely underestimated throughout the year in the absence of the OA coating

488   status effect (NOA).

489

490
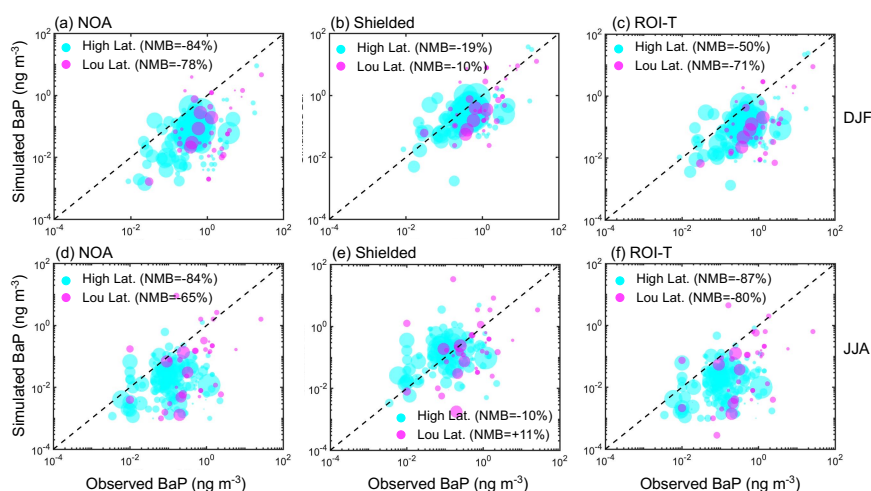
491   **Figure 6. Comparison between simulated surface BaP concentrations at relatively high latitude regions**

492   **(marked as olive, measured locations north of 40°N) and low latitude regions (marked as magenta, measured**

493   **locations between 40°N and 40°S) in (a-c) DJF and (d-f) JJA, respectively. The circle area is proportional to**

494   **the number of days sampled at each site. Both background and urban sites are included.**

495

496   In Europe, although the simulated BaP for the Shielded approach also exhibits the best agreement with

497   observations at 18 sites throughout the year, with a NMB of +16%, the simulated BaP fails to capture

498   the magnitude of the measured BaP concentrations during the warm season (Fig. 5f). From April to

499   October, model-predicted BaP concentrations in the Shielded simulation are overestimated by 88%. In

500   contrast, the simulated BaP concentrations for the ROI-T approach are consistent with the monthly

501   variation of the measured BaP concentrations, despite showing a 66% underestimated annual mean,

502   which is mainly due to the significant underestimation in cool season. Our results suggest that while the

503   Shielded simulation is likely closer to actual BaP magnitudes at mid- and low-latitudes, the ROI-T

504   approach may better represent seasonal variation at mid-and high-latitudes but overestimates the

505   coefficient of BaP multiphase degradation rates.

506 **3.3.2 Oxidized BaP**

507 Due to limited observations of oxidized BaP, specifically 1-, 3-, and 6-nitrobenzo(a)pyrene, we assess
508 monthly changes in BaP for three different particle-bound BaP degradation approaches performed at two
509 sites, Grenoble and SIRTA. In this study, we compare both simulated fresh BaP and oxidized BaP with
510 in situ measurements. For Grenoble, we use downscaled simulated fresh/oxidized BaP concentrations
511 for comparison, while at the SIRTA site, we compare coarse-resolution simulated BaP concentrations
512 with measurements.

513
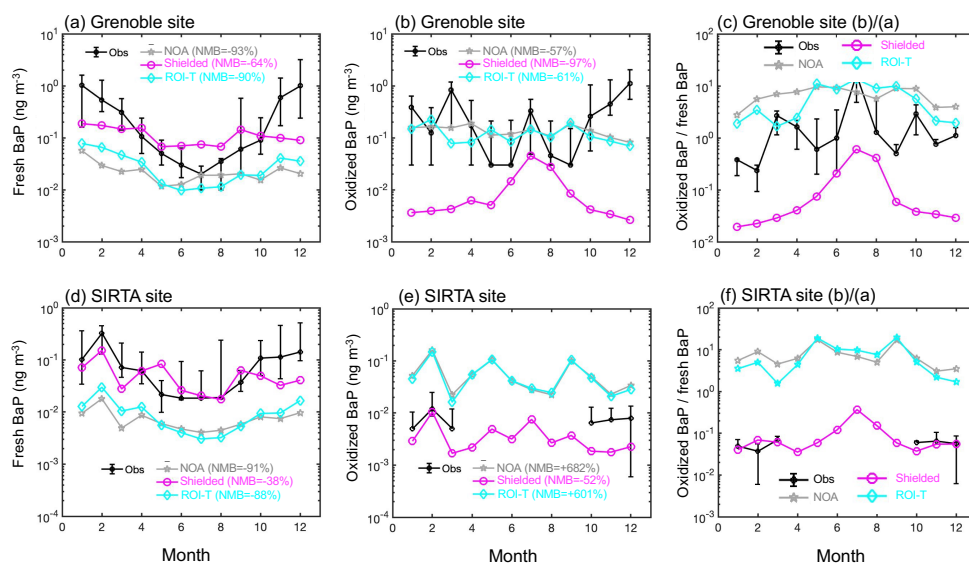
514
515 **Figure 7. Monthly comparison between simulated surface fresh and oxidized BaP from NOA, Shielded, and**
516 **ROI-T simulations and ground-based measurements at (a-c) Grenoble and (d-f) SIRTA sites. Black lines**
517 **represent measured values (median and 15th and 85th percentiles of each site), while blue (NOA), red**
518 **(Shielded), and green (ROI-T) lines represent the model-simulated median per month. The ratio of oxidized**
519 **BaP to fresh BaP is represent in (c) and (f). From April to September at the SIRTA site, observed**
520 **concentrations of oxidized BaP were below LQ and therefore not presented on the graph.**

521

522 The measurement site at the sampling station of "Les Frenes" in Grenoble (5.73ºE, 45.16ºN, France)
523 represents the most densely populated urban area in Europe. Although the simulated concentrations
524 applying the Shielded approach best match the observed fresh BaP concentrations in Grenoble among
525 the three approaches, the model largely underestimates winter BaP concentrations but overestimates
526 summer concentrations (Fig. 7a). Therefore, the assumption that viscous organic aerosol coatings
527 completely shut off the reaction of fresh particle-bound BaP with ozone under cool and dry conditions
528 is somewhat distorted and fails to capture seasonal variation in fresh BaP in Grenoble. The relatively low
529 ratio of oxidized to fresh BaP using the Shielded approach in Fig. 7c indicates that the chemical scheme
530 overly protects fresh PAHs from oxidation. Consequently, it underestimates oxidized BaP by one order
531 of magnitude. In contrast, despite the overall underestimation, the ROI-T simulation captures the
532 seasonal variations in fresh BaP concentrations in Grenoble (Fig. 7a). However, the magnitude of the
533 simulated oxidized BaP concentration is very similar to the observed values (Fig. 7b). As we mentioned

534 above, the ratio of oxidized to fresh BaP in Fig. 7c reveals that the oxidation rate of BaP from fresh to
535 oxidized is too fast under ROI-T treatment, especially during cold season.
536 In addition, the underestimation of both fresh and oxidized BaP concentrations may be partly due to the
537 coarse horizontal resolution of simulated BaP, and inaccurate urban PAH emissions. We use a
538 downscaling formulation to convert the 200 km grid resolution to a ~10 km grid resolution, but the spatial
539 distribution of BaP obtained in this way is highly dependent on accurate emissions and meteorological
540 fields. Previous studies have reported that traditional biomass combustion for residential heating is the
541 main source of $PM_{2.5}$ in France in winter and including in the Grenoble area [Favez et al., 2009; 2021;
542 Srivastava et al., 2018; Weber et al., 2019; Zhang et al., 2020a], thus inevitably emitting large amounts
543 of BaP. Considering the underestimation of both fresh and oxidized BaP concentrations at the Grenoble
544 site in winter, there is a large uncertainty in the emission and spatial distribution of PAHs in urban areas
545 (Fig. 7a, b).
546 For the SIRTA site, the simulated BaP from the Shielded simulation shows good performance compared
547 to the observed concentrations of fresh and oxidized BaP in winter (Fig. 7d, e). The performance of
548 Shielded approach in summer remains unclear due to the lack of observed concentrations of oxidized
549 BaP (Fig. 7e). However, the underestimation of fresh BaP concentrations and overestimation of oxidized
550 BaP concentrations in ROI-T and NOA suggest that the particle-bound PAH degradation rate is too fast
551 for these two approaches (Fig. 7c-d).
552 According to the ROI-T approach, once BaP is absorbed by organic aerosols, it can only be oxidized
553 when it comes to the surface through bulk diffusion or O_3 absorption from the gas sorption layer to bulk
554 layers. The changes in the BaP degradation rate coefficient are highly dependent on variations in
555 temperature and relative humidity [Mu et al., 2018]. Considering that RH in the French winter is
556 generally higher than 70% (Fig. 2b), the BaP degradation rate coefficient decreases by only one order of
557 magnitude for every 20 K drop in temperature from around 293 K (Table S1). Therefore, the oxidation
558 rate of ROI-T for particle-bound PAHs is reduced by no more than 50% when the temperature is around
559 280 K in the French winter (Fig. 2a). Our results suggest that at higher humidity, the ROI-T approach
560 underestimates the impact of OA coatings on PAH degradation effectiveness. Thus, the model's ability
561 to simulate fresh BaP is not significantly enhanced over the default NOA when the ROI-T approach is
562 selected, as relative humidity is significantly higher than 70% in mid- and high-latitude winters (Figs. 5f,
563 6c).

564 **3.4. Lung-cancer risk of PAH mixture**

565 As an indicator of cancer risk from PAH mixtures, previous studies calculated PAH-associated health
566 risks based on exposure to BaP concentrations using a method grounded in epidemiological data
567 [Bostrom et al., 2002; Zhang et al., 2009; Shen et al., 2014; Shrivastava et al., 2017; T Wang et al., 2017;
568 Kelly et al., 2021]. These studies primarily considered fresh PAHs when assessing PAH-associated
569 health risks. In this study, we follow the approach of previous studies to estimate ILCR [Shen et al., 2014;
570 Shrivastava et al., 2017; Lou et al., 2023].
571 Figure 8a illustrates that global and regional population-weighted ILCR varies significantly across
572 simulations when only considering exposure to fresh PAH. This variation is due to the substantial impact
573 of PAH degradation approaches on fresh BaP concentrations. On a global population-weighted basis, the

574 ILCR is predicted to be ~0.6×10^{-5} from the NOA and ROI-T simulations, falling within WHO-acceptable

575 risk levels for PAH exposure. However, based on the Shielded simulation, the global population-

576 weighted ILCR is predicted to be ~2×10^{-5}, exceeding the acceptable limit of 1 death per 100,000 persons.

577 Moreover, without the heterogeneous oxidation of BaP, Shen et al. (2014) predicted an even higher

578 global population-weighted ILCR of 3×10^{-5}. These results underscore the high sensitivity of global ILCR

579 estimates to the choice of PAH degradation approaches.

580 The variations in fresh BaP exposure and population-weighted ILCR are even more important for

581 regional estimation. Using the Shielded approach, the regional average population-weighted ILCR is

582 predicted to exceed 1×10^{-5} over East Asia, South Asia, Southeast Asia, Russia, Africa, and South

583 America. In contrast, ILCR for NOA and ROI-T simulations suggests a 3-4 times lower lung cancer risk

584 in these regions, expected to be below 1×10^{-5} except in East Asia (Fig. 8a). Due to the high emission

585 levels in 2008, the ROI-T simulation estimates a 50% higher ILCR than the NOA simulation, also

586 exceeding the WHO acceptable limit in the East Asia.

587 Furthermore, recent laboratory studies suggest that oxidized PAHs persist in the particle-phase and often

588 appear as higher molecular weight peaks in particle mass spectra [Ringuet et al., 2012; Zelenyuk et al.,

589 2012; Keyte et al., 2013; Jariyasopit et al., 2014]. Some PAH oxidation products may even be more toxic

590 than their parent compounds [EHC 2003; Clergé et al., 2019; Hrdina et al., 2022; Peng et al., 2023]. A

591 quantitative understanding of the toxicity of these products is lacking, as each parent PAH could be

592 oxidized into hundreds of products. In this study, we conduct a conservative first-order calculation of

593 lung cancer risk associated with oxidized PAHs, assuming that PAH oxidation products have the same

594 toxicity as their parents. On a global population-weighted basis, the ILCR is projected to 2.5 deaths per

595 100,000 persons when exposure to oxidized BaP is added to our previous calculations of fresh BaP

596 exposure for all three simulation approaches (Fig. 8b). While three-quarters of the global population-

597 weighted ILCR for the Shielded simulation is contributed to fresh PAH, oxidized PAHs contribute

598 approximately 40% the ILCR in warm and humid regions such as South Asia, Southeast Asia, and Africa.

599 In comparison, NOA and ROI-T simulations predict a dominant contribution of ILCR from PAH

600 oxidation products compared to fresh PAHs over most regions of the globe. For example, over East Asia

601 and South Asia, the NOA and ROI-T simulations predict that the regional population-weighted ILCR

602 will exceed 3 deaths per 100,000 persons resulting from the oxidized PAHs alone, compared to ~1 death

603 per 100,000 persons from oxidized PAHs in the Shielded simulation. The oxidized-fresh PAH ILCR split

604 is much greater in the NOA and ROI-T simulations compared to the Shielded simulation.

605 Despite differences in organic coating effectiveness and heterogeneous reactivity between the NOA,

606 Shielded, and ROI-T simulations, all schemes suggest that oxidized PAHs are crucial for lung cancer

607 risk and cannot be neglected. If the toxicity of oxidized PAHs is similar to fresh PAHs, the total ILCR

608 (fresh+oxidized) is comparable in the three approaches. However, oxidized PAHs could be much more

609 important in certain regions (such as Southeast Asia, South Asia, and Africa), depending on their

610 composition/toxicity and where the organic coatings are less effective in shielding them from

611 heterogeneous reactivity. Considering the high levels of oxidized PAHs in mid-to-low latitudes, the

612 measurements for oxidized PAHs, as well as human health exposure to oxidized PAHs, are necessary

613 for further studies [Kelly et al., 2021].

614

615
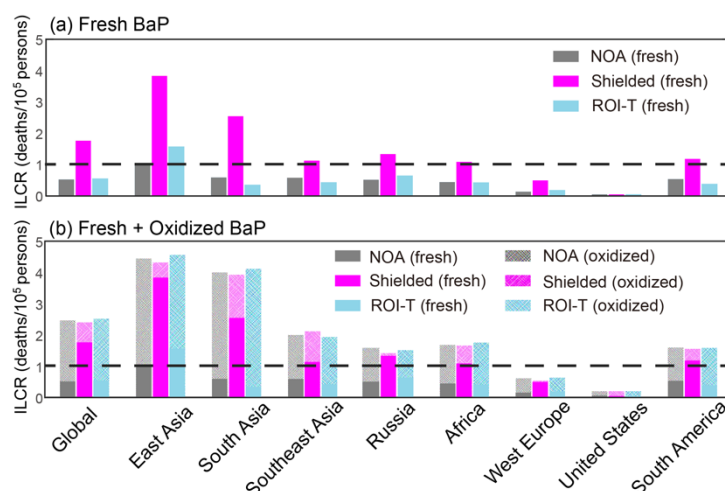
Figure 8. Regional PAH-associated ILCR from NOA, Shielded, and ROI-T simulations. Note that solid bars in (a, b) and shaded bars in (b) represent ILCR calculated from exposure to fresh and oxidized PAHs, respectively.

616
617
618

619 **4. Conclusion and Discussion**

620 This study uses the CAM5 model to investigate the impact of particle-bound PAH degradation
621 approaches on the spatial distribution of BaP, considering the presence or absence (or lack of effect) of
622 OA coatings. The three PAH degradation approaches are (1) no effect of OA coating state (e.g., thickness)
623 on BaP oxidation (NOA), (2) thick OA coatings (> 20 nm thick) completely shielding particle-bound
624 BaP oxidation under cool, dry conditions (Shielded), and (3) OA coatings slowing down particle-bound
625 BaP oxidization in response to temperature and humidity (ROI-T). The results show significant seasonal
626 variations in BaP concentrations driven by emissions, deposition, and the chosen degradation approach.
627 In DJF, without the viscous OA coatings, the model severely underestimates the global fresh BaP
628 concentration (PWGA=0.24 ng m^{-3}), as 82% of the BaP is oxidized near source areas. Including viscous
629 OA coatings substantially slows oxidation, leading to 2-6 times higher fresh BaP concentrations. Notably,
630 the Shielded approach predicts the highest BaP concentration. While the Shielded and ROI-T approaches
631 predict similar fresh BaP distributions at high latitudes, the ROI-T approach suggests faster
632 heterogeneous degradation kinetics of BaP with ozone at warm temperatures (>288K, see Table S1),
633 resulting in lower predicted BaP concentrations in regions such as Africa, South Asia, and East Asia.
634 In JJA, BaP concentrations are concentrated near source areas. The Shielded approach continues to
635 predict higher fresh BaP concentrations than simulations without viscous OA coatings, while the ROI-T
636 approach predicts the lowest concentrations due to faster oxidation under warmer, more humid
637 conditions. Over 90% of BaP is oxidized in the tropics (30°S-30°N) in all simulations. At mid-to-high
638 latitudes, oxidation rates vary greatly depending on OA coating assumptions. In the Shielded simulation,
639 only 40% of BaP is oxidized, compared to 91% in the NOA and 94% in the ROI-T simulations.
640 Model performance is compared with observations at 66 background/remote and 208 non-background
641 sites globally. The NOA and ROI-T simulations perform poorly, underestimating fresh BaP
642 concentrations by 60-80%. However, the Shielded approach agrees best with observations, with a NMB
643 consistently within ±20%. Both the Shielded and ROI-T approaches improve BaP concentrations and

644 seasonal variations in China. While the Shielded approach aligns more closely with BaP concentrations

645 in Europe, it fails to capture seasonal variation in fresh BaP. Additionally, oxidized BaP concentrations

646 from Grenoble (2013) and SIRTA (2014-2015) are also used for model evaluation. Our results indicate

647 that the Shielded approach underestimates BaP oxidation rates, particularly in the warm season, while

648 the ROI-T approach overpredicts oxidation rates in multiple regions but better represents seasonal

649 variations in fresh BaP concentrations.

650 Epidemiological data are used to estimate the population-weighted ILCR associated with PAH exposure.

651 For fresh BaP alone, the PWGA ILCR ranges from $\sim 0.6 \times 10^{-5}$ to $\sim 2 \times 10^{-5}$ among the three simulations,

652 exceeding the acceptable limit of 1 death per 100,000 persons when considering the effect of viscous OA

653 coatings. When both fresh and oxidized PAHs are assumed to equally contribute to cancer risk, the total

654 ILCR remains comparable across all simulations, amounting to 2.5 deaths per 100,000 persons. This is

655 because the combined concentration of fresh and oxidized BaP is similar across the three simulations.

656 This highlights the potential significance of oxidized PAHs, particularly in regions where they may play

657 a substantial role in health risks.

658 This study highlights the importance of understanding the effects of viscous OA coatings on BaP

659 degradation. However, the approaches used in this study have limitations that need to be addressed in

660 future research, to better improve global PAH simulations. The viscosity of OA affects BaP degradation

661 in two ways: (1) through gas-particle partitioning of SOA, and (2) by altering BaP degradation kinetics

662 with ozone. In terms of gas-particle partitioning, viscosity is treated differently in each approach. In the

663 NOA simulation (section 2.3), the FragSVSOA treatment is used, which assumes SOA remains a semi-

664 volatile, liquid-like solution throughout its lifetime, without considering the effect of its viscosity on gas-

665 particle partitioning. In contrast, the Shielded and ROI-T approaches use the FragNVSOA treatment,

666 which assumes that SOA rapidly transitions to a highly viscous, non-volatile semi-solid within 30

667 minutes due to paricle-phase oligomerization reactions [Shrivastava et al., 2015]. Any further gas-phase

668 organic oxidation products do not form a solution with pre-existing OA. This assumption aligns with a

669 recent experimental study showing that isoprene SOA undergoes rapid aging (~20 minutes), leading to

670 oligomer and organosulfate formation and a phase transition to semi-solid SOA [Chen et al. 2023].

671 Regarding the second effect, both the Shielded and ROI-T approaches incorporate the effect of SOA

672 viscosity on BaP degradation kinetics with ozone. The Shielded approach, based on Shrivastava et al.

673 (2017), assumes that thick OA coatings completely shield particle-bound BaP oxidation under cool

674 (temperature < 296 K) and dry (RH < 50%) conditions, thus providing an upper bound of the impact of

675 viscous SOA on BaP degradation and underestimating the oxidation rate, particularly in urban areas. The

676 ROI-T approach models the multiphase degradation of BaP with ozone, incorporates both mass transport

677 and chemical reactions of particle-bound species in the bulk phase and at the surface. The first-order

678 decay rates of BaP, as presented in Table S3 of Mu et al. (2018), are parameterized values that already

679 account for the impact of changing SOA viscosity as a function of temperature and RH on BaP

680 degradation, although this may overestimate the oxidation rate in remote area (Fig. 7).

681 Both the Shielded and ROI-T approaches assume a globally constant 30-minute timescale for the

682 transformation of SOA to a semi-solid state, which aligns with a recent experimental study [Chen et al.

683 2023]. However, future studies are needed to measure the phase transition timescale of different SOA

684 types under varying temperature and relative humidity conditions. Previous modelling studies have

685 suggested that the phase state of OA varies significantly with environmental factors such as temperature,

RH in different SOA systems [Pye et al., 2017; Shiraiwa et al., 2017; Zhang et al., 2019; Li et al., 2020; Schmedding et al., 2020]. In addition, water associated with organics has been suggested to be the primary predictor of OA viscosity [Rasool et al., 2021]. The effects of phase separation within SOA-water mixtures and variability in the water uptake ability of SOA as a function of its aging and gas-particle partitioning, and the resulting impacts on SOA viscosity and BaP reaction kinetics need to be considered in future studies.

The pp-LFER approach used in our study considers the effects of BaP partitioning to a two-phase organic system consisting of liquid water-soluble/organic soluble organics, and solid/semisolid organic polymers. In this sense, this approach considers the impacts of water-soluble organics and organic polymers (formed by accretion reactions) on BaP partitioning. Further experiments that measure the partitioning of BaP on liquid-like SOA and polymeric SOA systems are needed to constrain pp-LFER model predictions.

To improve global PAH simulations, future research should focus on understanding the impact of OA coatings on PAH degradation effectiveness, particularly incorporating the variations in phase-state of OA coatings in models. Expanding the observational dataset to include a wider range of ground-based and satellite-derived measurements, such as water-soluble organic aerosols (Zhang et al., 2020b), will also be crucial for validating and refining these models. Additionally, further exploration of the chemical composition and toxicity of both fresh and oxidized PAHs is necessary to assess their role in air quality and human health risk more effectively.

Data availability

The ERA-Interim reanalysis data is available from https://www.ecmwf.int/en/forecasts/datasets/reanalysis-datasets/era-interim. The GEMS 0.1º × 0.1º global BaP emission inventory is available from gems.sustech.edu.cn. The long-term observation data are obtained from IADN (https://www.epa.gov/great-lakes-monitoring/great-lakes-integrated-atmospheric-deposition-network), EMEP (https://www.emep.int), and GENASIS (https://www.genasis.cz).

Acknowledgments

This research was supported by the National Natural Science Foundation of China (grant number: 42075095), Fundamental Research Funds for the Central Universities (grant number: 14380198), the Energy Exascale Earth System Model (E3SM) project. Manish Shrivastava was supported by the U.S. Department of Energy (DOE) Office of Science, Office of Biological and Environmental Research (BER) through the Early Career Research programme and DOE BER's Atmospheric System Research (ASR) program. The Pacific Northwest National Laboratory (PNNL) is operated for DOE by Battelle Memorial Institute under Contract DE-AC05-76RL01830. This work was also supported by the French Ministry of environment and the National reference laboratory for air quality monitoring in France (LCSQA).

References

Ahad, J. M. E., Macdonald, R. W., Parrott, J. L., Yang, Z., Zhang, Y., Siddique, T., Kuznetsova, A., Rauert, C., Galarneau, E., Studabaker, W. B., Evans, M., McMaster, M. E., Shang, D.: Polycyclic aromatic compounds (PACs) in the Canadian environment: A review of sampling techniques, strategies and instrumentation, Environ. Pollut., 266(Pt 2), 114988, doi: https://doi.org/10.1016/j.envpol.2020.114988, 2020.

Arp, H. P., Schwarzenbach, R. P., and Goss, K. U.: Ambient gas/particle partitioning. 2: The influence of particle source and temperature on sorption to dry terrestrial aerosols, Environ. Sci. Technol., 42(16), 5951-5957, https://doi.org/10.1021/es703096p, 2008.

Berkemeier, T., Steimer, S. S., Krieger, U. K., Peter, T., Poschl, U., Ammann, M., and Shiraiwa, M.: Ozone uptake on glassy, semi-solid and liquid organic matter and the role of reactive oxygen intermediates in atmospheric aerosol chemistry, Phys. Chem. Chem. Phys., 18(18), 12662-12674, https://doi.org/10.1039/C6CP00634E, 2016.

Bateman, A. P., Bertram, A. K., and Martin, S. T.: Hygroscopic influence on the semisolid-to-liquid transition of secondary organic materials, J. Phys. Chem. A, 119(19), 4386-4395, dx.doi.org/10.1021/jp508521c, 2015.

Boffetta, P., Jourenkova, N., and Gustavsson, P.: Cancer risk from occupational and environmental exposure to polycyclic aromatic hydrocarbons, Cancer Causes & Control, 8(3), 444-472, doi:10.1023/a:1018465507029, 1997.

Boruvkova, J.: GENASIS-Global Environmental Assessment and Information System, version 2.0., Masaryk University, www.genasis.cz, 2015.

Bostrom, C. E., Gerde, P. , Hanberg, A., Jernstrom, B., Johansson, C., Kyrklund, T., Rannug, A., Tornqvist, M., Victorin, K., and Westerholm, R.: Cancer risk assessment, indicators, and guidelines for polycyclic aromatic hydrocarbons in the ambient air, Environ. Health Perspect., 110, 451-488, doi:10.1289/ehp.110-1241197, 2002.

Brown, A. S., Brown, R. J., Coleman, P. J., Conolly, C., Sweetman, A. J., Jones, K. C., Butterfield, D. M., Sarantaridis, D., Donovan, B. J., and Roberts, I.: Twenty years of measurement of polycyclic aromatic hydrocarbons (PAHs) in UK ambient air by nationwide air quality networks, Environ Sci: Process. Impacts., 15(6), doi:10.1039/c3em00126a, 1199-1215, 2013.

Cazaunau, M., Ménach, K. Le, Budzinski, H., and Villenave, E.: Atmospheric heterogeneous reactions of Benzo(a)pyrene, Z. für Phys. Chem., 224, 1151-1170, https://doi.org/10.1524/zpch.2010.6145, 2010.

CA EPA. Technical support document for cancer potency factors: methodologies for derivation, listing of available values, and adjustments to allow for early life stage exposures https://oehha.ca.gov/media/downloads/crnr/tsdcancerpotency.pdf, 2009. (last accessed 4 Feb. 2025)

Chen, S.-C., and Liao, C.-M.: Health risk assessment on human exposed to environmental polycyclic aromatic hydrocarbons pollution sources, Sci. Total Environ., 366(1), 112-123, https//doi.org/10.1016/j.scitotenv.2005.08.047, 2006.

Chen, Y., Zaveri, R. A., Vandergrift, G. W., Cheng, Z., China, S., Zelenyuk, A., and Shilling, J. E.: Nonequilibrium behavior in isoprene secondary organic aerosol, Environ. Sci. Technol., 57, 38, 14182-14193, https://doi.org/10.1021/acs.est.3c03532, 2023.

Clergé, A., Le Goff, J., Lopez, C., Ledauphin, J., and Delépée, R.: Oxy-PAHs: occurrence in the environment and potential genotoxic/mutagenic risk assessment for human health, Critical reviews in toxicology, 49(4), 302-328, doi:10.1080/10408444.2019.1605333, 2019.

CPCB (Central Pollution Control Board): National Ambient Air Quality Monitoring Programme (NAAQMS) Report No. 45/2019-2020, Ministry of Environment, Forest and Climate Change, Government of India, New Delhi, India, 2020.

Crippa, M., Guizzardi, D., Muntean, M., Schaaf, E., Dentener, F., van Aardenne, J. A., Monni, S., Doering, U., Olivier, J. G. J., Pagliari, V., and Janssens-Maenhout, G: Gridded emissions of air pollutants for the period 1970-2012 within EDGAR v4.3.2, Earth Syst. Sci. Data, 10(4), 1987-2013, https://doi.org/10.5194/essd-10-1987-2018, 2018.

Emmons, L. K., Walters, S., Hess, P. G., Lamarque, J.-F., Pfister, G. G., Fillmore, D., Granier, C., Guenther, A., Kinnison, D., Laepple, T., Orlando, J., Tie, X., Tyndall, G., Wiedinmyer, C., Baughcum, S. L., and Kloster, S.: Description and evaluation of the Model for Ozone and Related chemical Tracers, version 4 (MOZART-4), Geosci. Model Dev., 3(1), 43-67, https://doi.org/10.5194/gmd-3-43-2010, 2010.

HEC (Environmental Health Criteria) 229: Selected nitro- and nitro-oxy-polycyclic aromatic hydrocarbons, WHO Library, https://www.inchem.org/documents/ehc/ehc/ehc229.htm, 2003.

EPA (Environmental Protection Agency): Air Quality Criteria for Particulate Matter (EPA/600/P-99/002aF, EPA/600/P-99/002bF), Office of Research and Development, Washington, DC, USA, 2004.

EPCEU (European Parliament and Council of the European Union): Directive 2004/107/EC of the European Parliament and of the Council of 15 December 2004 relating to arsenic, cadmium, mercury, nickel and polycyclic aromatic hydrocarbons in ambient air, Official Journal of the European Union, L23, 3-16, 2004.

Esteve, W., Budzinski, H., and Villenave, E.: Relative rate constants for the heterogeneous reactions of NO and OH radicals with polycyclic aromatic hydrocarbons adsorbed on carbonaceous particles. Part 2: PAHs adsorbed on diesel particulate exhaust SRM 1650a, Atmos. Environ., 40(2), 201-211, https://doi.org/10.1016/j.atmosenv.2005.07.053, 2006.

Famiyeh, L., Chen, K., Xu, J., Sun, Y., Guo, Q., Wang, C., Lv, J., Tang, Y.-T., Yu, H., Snape, C., He, J.: A review on analysis methods, source identification, and cancer risk evaluation of atmospheric polycyclic aromatic hydrocarbons, Sci. Total. Environ., 789, 147741, https://doi.org/10.1016/j.scitotenv.2021.147741, 2021.

Favez, O., Cachier, H., Sciare, J., Sarda-Estève, R., and Martinon L.: Evidence for a significant contribution of wood burning aerosols to PM during the winter season in Paris, France, Atmos. Environ., 43(22-23), 3640-3644, https://doi.org/10.1016/j.atmosenv.2009.04.035, 2009.

Favez, O., Weber, S., Petit, J.-E., Alleman, L. Y., Albinet, A., Riffault, V., Chazeau, B., Amodeo, T., Salameh, D., Zhang, Y., Srivastava, D., Samaké, A., Aujay-Plouzeau, R., Papin, A., Bonnaire, N., Boullanger, C., Chatain, M., Chevrier, F., Detournay, A., Dominik-Sègue, M., Falhun, R., Garbin, C., Ghersi, V., Grignion, G., Levigoureux, G., Pontet, S., Rangognio, J., Zhang, S., Besombes, J.-L., Conil, S., Uzu, G., Savarino, J., Marchand, N., Gros, V., Marchand, C., Jaffrezo, J.-L., and Leoz-Garziandia, E.: Overview of the French Operational Network for In Situ Observation of PM Chemical Composition and Sources in Urban Environments (CARA Program), Atmosphere, 12, 207, https://doi.org/10.3390/atmos12020207, 2021.

805 Friedman, C. L., Pierce, J. R., and Selin, N. E.: Assessing the influence of secondary organic versus
806 primary carbonaceous aerosols on long-range atmospheric polycyclic aromatic hydrocarbon transport,
807 Environ Sci Technol, 48(6), 3293-3302, https://doi.org/10.1021/es405219r, 2014.

808 Friedman, C. L. and Selin, N. E.: Long-range atmospheric transport of polycyclic aromatic
809 hydrocarbons: A global 3-D model analysis including evaluation of Arctic sources, Environ. Sci.
810 Technol., 46(17), 9501-9510, https://doi.org/10.1021/es301904d, 2012.

811 Galarneau, E., Makar, P. A., Zheng, Q., Narayan, J., Zhang, J., Moran, M. D., Bari, M. A., Pathela, S.,
812 Chen, A. and Chlumsky, R.: PAH concentrations simulated with the AURAMS-PAH chemical transport
813 model over Canada and the USA, Atmos. Chem. Phys., 14(8), 4065-4077, https://doi.org/10.5194/acp-
814 14-4065-2014, 2014.

815 Halsall, C. J., Barrie, L. A., Fellin, P., Muir, D. C. G., Billeck, B. N., Lockhart, L., Rovinsky, F. Y., .
816 Kononov, E. Y., and Pastukhov, B.: Spatial and temporal variation of polycyclic aromatic hydrocarbons
817 in the Arctic atmosphere, Environ. Sci. Technol., 31(12), 3593-3599, https://doi.org/10.1021/es970342d,
818 1997.

819 Han, F., Guo, H., Hu, J., Zhang, J., Ying, Q., and Zhang, H.: Sources and health risks of ambient
820 polycyclic aromatic hydrocarbons in China, Sci. Total Environ., 698, 134229,
821 https://doi.org/10.1016/j.scitotenv.2019.134229, 2020.

822 Han, F., Kota, S. H., Sharma, S., Zhang, J., Ying, Q., and Zhang, H.: Modeling polycyclic aromatic
823 hydrocarbons in India: Seasonal variations, sources and associated health risks, Environ Res, 212(Pt D),
824 113466, https://doi.org/10.1016/j.envres.2022.113466, 2022.

825 Han, J., Liang, Y. S., Zhao, B., Wang, Y., Xing, F. T., and Qin, L. B.: Polycyclic aromatic hydrocarbon
826 (PAHs) geographical distribution in China and their source, risk assessment analysis, Environ. Pollut.,
827 251, 312-327, https://doi.org/10.1016/j.envpol.2019.05.022, 2019.

828 Hrdina, A. I. H., Kohale, I. N., Kaushal, S., Kelly, J., Selin, N. E., Engelward, B. P., and Kroll, J. H.:
829 The parallel transformations of polycyclic aromatic hydrocarbons in the body and in the
830 atmosphere, Environ. Health Perspect., 130(2), 025004, https://doi.org/10.1289/EHP9984, 2022.

831 Hu, R., Liu, G., Zhang, H., Xue, H., and Wang, X.: Levels and Sources of PAHs in Air-borne PM(2.5)
832 of Hefei City, China, Bull. Environ. Contam. Toxicol., 98(2), 270-276, doi:10.1007/s00128-016-2019-
833 9, 2017.

834 Hu, R., Liu, G., Zhang, H., Xue, H., Wang, X., and Wang, R.: Particle-Associated Polycyclic Aromatic
835 Hydrocarbons (PAHs) in the Atmosphere of Hefei, China: Levels, Characterizations and Health Risks,
836 Arch. Environ. Contam. Toxicol., 74(3), 442-451, doi:10.1007/s00244-017-0472-z, 2018.

837 Hung, H., Kallenborn, R., Breivik, Knut, Su, Y., Brorström-Lundén, E., Olafsdottir, K., Thorlacius, J.
838 M., Leppänen, S., Bossi, R., Skov, H., Manø, S., Patton, G. W., Stern, G., Sverko, E., and Fellin, P.:
839 Atmospheric monitoring of organic pollutants in the Arctic under the Arctic Monitoring and Assessment
840 Programme (AMAP): 1993-2006, Sci. Total Environ., 408(15), 2854-2873,
841 doi:10.1016/j.scitotenv.2009.10.004, 2010.

842 IARC: Some non-heterocyclic polycyclic aromatic hydrocarbons and some related exposures, IARC
843 Monographs on the Evaluation of Carcinogenc Risks to Humans, 92, 1-853, ISBN-13, 978-92-832-1292-
844 8, 978-92-832-1292-9, 2010.

845   IARC: International Agency for Research on Cancer (IARC) monographs on the identification of
846   carcinogenic hazards to humans, Agents Classified by the IARC Monographs,
847   https://monographs.iarc.who.int/list-of-classifications, 2021.

848   Iakovides, M., Apostolaki, M., and Stephanou, E. G.: PAHs, PCBs and organochlorine pesticides in the
849   atmosphere of Eastern Mediterranean: Investigation of their occurrence, sources and gas-particle
850   partitioning in relation to air mass transport pathways, Atmos. Environ., 244, 117931,
851   https://doi.org/10.1016/j.atmosenv.2020.117931, 2021.

852   Janssens-Maenhout, G., Crippa, M., Guizzardi, D., Dentener, F., Muntean, M., Pouliot, G., Keating, T.,
853   Zhang, Q., Kurokawa, J., Wankmüller, R., van der Gon, H. D., Kuenen, J. J. P., Klimont, Z., Frost, G.,
854   Darras, S., Koffi, B., and Li, M.: HTAP_v2.2: a mosaic of regional and global emission grid maps for
855   2008 and 2010 to study hemispheric transport of air pollution, Atmos. Chem. Phys., 15(19), 11411-
856   11432, https://doi.org/10.5194/acp-15-11411-2015, 2015.

857   Jariyasopit, N., McIntosh, M., Zimmermann, K., Arey, J., Atkinson, R., Cheong, P. H., Carter, R. G.,
858   Yu, T. W., Dashwood, R. H., and Massey Simonich, S. L.: Novel nitro-PAH formation from
859   heterogeneous reactions of PAHs with NO2, NO3/N2O5, and OH radicals: prediction, laboratory studies,
860   and mutagenicity, Environ. Sci. Technol., 48(1), 412-419, https://doi.org/10.1021/es4043808, 2014.

861   Kahan, T. F., Kwamena, N. O. A., and Donaldson D. J.: Heterogeneous ozonation kinetics of polycyclic
862   aromatic hydrocarbons on organic films, Atmos. Environ., 40(19), 3448-3459,
863   https://doi.org/10.1016/j.atmosenv.2006.02.004, 2006.

864   Keith, L. H.: The source of US EPA's sixteen PAH priority pollutants, Polycyclic Aromatic Compounds,
865   35(2-4), 147-160, https://doi.org/10.1080/10406638.2014.892886, 2015.

866   Kelly, J. M., Ivatt, P. D., Evans, M. J., Kroll, J. H., Hrdina, A. I. H., Kohale, I. N., White, F. M.,
867   Engelward, B. P., and Selin, N. E.: Global Cancer Risk From Unregulated Polycyclic Aromatic
868   Hydrocarbons, Geohealth, 5(9), e2021GH000401, https://doi.org/10.1029/2021GH000401, 2021.

869   Keyte, I. J., Harrison, R. M., and Lammel, G.: Chemical reactivity and long-range transport potential of
870   polycyclic aromatic hydrocarbons--a review, Chem. Soc. Rev., 42(24), 9333-9391,
871   https://doi.org/10.1039/C3CS60147A, 2013.

872   Kim, J. Y., Lee, J. Y., Choi, S. D., Kim, Y. P., and Ghim, Y. S.: Gaseous and particulate polycyclic
873   aromatic hydrocarbons at the Gosan background site in East Asia, Atmos. Environ., 49, 311-319,
874   https://doi.org/10.1016/j.atmosenv.2011.11.029, 2012.

875   Kim, K.-H., Jahan, S. A., Kabir, E., and Brown, R. J. C.: A review of airborne polycyclic aromatic
876   hydrocarbons (PAHs) and their human health effects, Environment International, 60, 71-80,
877   https://doi.org/10.1016/j.envint.2013.07.019, 2013.

878   Koop, T., Bookhold, J., Shiraiwa, M., and Poschl, U.: Glass transition and phase state of organic
879   compounds: dependency on molecular properties and implications for secondary organic aerosols in the
880   atmosphere, Phys. Chem. Chem. Phys., 13(43), 19238-19255, doi:10.1039/c1cp22617g, 2011.

881   Kumar, A., Sankar, T. K., Sethi, S. S., and Ambade, B.: Characteristics, toxicity, source identification
882   and seasonal variation of atmospheric polycyclic aromatic hydrocarbons over East India, Environ. Sci.
883   Pollut. Res. Int., 27(1), 678-690, doi:10.1007/s11356-019-06882-5, 2020.

884   Kwamena, N. O. A., Thornton, J. A., and Abbatt, J. P. D.: Kinetics of surface-bound benzo[a]pyrene and
885   ozone on solid organic and salt aerosols, J. Phys. Chem. A, 108(52), 11626-11634,
886   https://doi.org/10.1021/jp046161x, 2004.

Lammel, G., Dvorská, A., Klánová, J., Kohoutek, J., Kukacka, P., Prokes, R., and Sehili, A. M.: Long-range Atmospheric Transport of Polycyclic Aromatic Hydrocarbons is Worldwide Problem - Results from Measurements at Remote Sites and Modelling, Acta. Chim. Slov., 62(3), 729-735, doi:10.17344/acsi.2015.1387, 2015.

Lanzafame, G. M., Srivastava, D., Favez, O., Bandowe, B. A. M., Shahpoury, P., Lammel, G., Bonnaire, N., Alleman, L. Y., Couvidat, F., Bessagnet, B., Albinet, A.: One-year measurements of secondary organic aerosol (SOA) markers in the Paris region (France): Concentrations, gas/particle partitioning and SOA source apportionment, Sci. Total Environ., 757, 143921, https://doi.org/10.1016/j.scitotenv.2020.143921, 2021.

Lee, J. Y., Kim, Y. P., and Kang, C. H.: Characteristics of the ambient particulate PAHs at Seoul, a mega city of Northeast Asia in comparison with the characteristics of a background site, Atmos. Res., 99(1), 50-56, https://doi.org/10.1016/j.atmosres.2010.09.029, 2011.

Lhotka, R., Pokorná, P., and Zíková, N.: Long-Term Trends in PAH Concentrations and Sources at Rural Background Site in Central Europe, Atmosphere, 10(11), 687, https://doi.org/10.3390/atmos10110687, 2019.

Li, Y., Day, D. A., Stark, H., Jimenez, J. L., and Shiraiwa, M.: Predictions of the glass transition temperature and viscosity of organic aerosols from volatility distributions, Atmos. Chem. Phys., 20, 8103-8122, 10.5194/acp-20-8103-2020, 2020.

Li, Y., Zhu, Y., Liu, W., Yu, S., Tao, S., and Liu, W.: Modeling multimedia fate and health risk assessment of polycyclic aromatic hydrocarbons (PAHs) in the coastal regions of the Bohai and Yellow Seas, Sci. Total Environ., 818, 151789, https://doi.org/10.1016/j.scitotenv.2021.151789, 2022.

Liu, X., Easter, R. C., Ghan, S. J., Zaveri, R., Rasch, P., Shi, X., Lamarque, J.-F., Gettelman, A., Morrison, H., Vitt, F., Conley, A., Park, S., Neale, R., Hannay, C., Ekman, A. M. L., Hess, P., Mahowald, N., Collins, W., Iacono, M. J., Bretherton, C. S., Flanner, M. G., and Mitchell, D.: Toward a minimal representation of aerosols in climate models: description and evaluation in the Community Atmosphere Model CAM5, Geosci. Model Dev., 5(3), 709-739, https://doi.org/10.5194/gmd-5-709-2012, 2012.

Liu, Y., Yan, C., Ding, X., Wang, X., Fu, Q., Zhao, Q., Zhang, Y., Duan, Y., Qiu, X., and Zheng, M.: Sources and spatial distribution of particulate polycyclic aromatic hydrocarbons in Shanghai, China, Sci. Total Environ., 584, 307-317, https://doi.org/10.1016/j.scitotenv.2016.12.134, 2017.

Lohmann, R., and Lammel, G.: Adsorptive and absorptive contributions to the gas-particle partitioning of polycyclic aromatic hydrocarbons: state of knowledge and recommended parametrization for modeling, Environ. Sci. Technol., 38(14), 3793-3803, https://doi.org/10.1021/es035337q, 2004.

Lou, S., Shrivastava, M., Ding, A., Easter, R. C., Fast, J. D., Rasch, P. J., Shen, H., Massey Simonich, S. L., Smith, S. J., and Tao, S.: Shift in Peaks of PAH‐Associated Health Risks From East Asia to South Asia and Africa in the Future, Earth's Future, 11(6), e2022EF003185, https://doi.org/10.1029/2022EF003185, 2023.

Ma, W.-L., Liu, L.-Y., Jia, H.-L., Yang, M., and Li, Y.-F.: PAHs in Chinese atmosphere Part I: Concentration, source and temperature dependence, Atmos. Environ., 173, 330-337, https://doi.org/10.1016/j.atmosenv.2017.11.029, 2018.

Masclet, P., Hoyau, V., Jaffrezo, J. L., and Cachier H.: Polycyclic aromatic hydrocarbon deposition on the ice sheet of Greenland. Part I: superficial snow, Atmos. Environ., 34, 3195-3207, https://doi.org/10.1016/S1352-2310(99)00196-X, 2000.

Matthias, V., Aulinger, A. and Quante, M.: CMAQ simulations of the benzo(a)pyrene distribution over Europe for 2000 and 2001, Atmos. Environ., 43(26), 4078-4086, https://doi.org/10.1016/j.atmosenv.2009.04.058, 2009.

MEPPRC (Ministry of Environmental Protection of the People's Republic of China): Water quality - Derermination of polycyclic aromatic hydrocarbons - Liquid-liquid extraction and solid-phase extraction followed by high performance liquid chromatographic method, Nathional Environmental Protection Standards HJ 478-2009, Beijing, China, pp1-10, in Chinese, 2009.

Mu, Q., Shiraiwa, M., Octaviani, M., Ma, N., Ding, A., Su, H., Lammel, G., Poschl, U., and Cheng, Y.: Temperature effect on phase state and reactivity controls atmospheric multiphase chemistry and transport of PAHs, Sci. Adv., 4(3), doi:10.1126/sciadv.aap7314, 2018.

Muir, D., Bossi, R., Carlsson, P., Evans, M., De Silva, A., Halsall, C., Rauert, C., Herzke, D., Hung, H., Letcher, R., Rigét, F., and Roos, A.: Levels and trends of poly- and perfluoroalkyl substances in the Arctic environment - An update, Emerg. Contam., 5, 240-271, https://doi.org/10.1016/j.emcon.2019.06.002, 2019.

Munyeza, C. F., Rohwer, E. R., and Forbes, P. B. C.: A review of monitoring of airborne polycyclic aromatic hydrocarbons: An African perspective, Trends Anal. Chem., 24, e00070, https://doi.org/10.1016/j.teac.2019.e00070, 2019.

Niu J., Sun, P., and Schramm, K.-W.: Photolysis of polycyclic aromatic hydrocarbons associated with fly ash particles under simulated sunlight irradiation, Journal of Photochemistry and Photobiology A: Chemistry, 186(1), 93-98, https://doi.org/10.1016/j.jphotochem.2006.07.016, 2007.

Peng, B., Dong, Q., Li, F., Wang, T., Qiu, X., and Zhu, T.: A systematic review of polycyclic aromatic hydrocarbon derivatives: occurrences, levels, biotransformation, exposure biomarkers, and toxicity, Environ. Sci. Technol., 57(41), 15314-15335, https://doi.org/10.1021/acs.est.3c03170, 2023.

Perera, F. P. J. S.: Environment and cancer: who are susceptible?, Science, 278(5340), 1068-1073, doi:10.1126/science.278.5340.1068, 1997.

Pöschl, U., Letzel, T., Schauer, C., and Niessner, R.: Interaction of ozone and water vapor with spark discharge soot aerosol particles coated with benzo [a] pyrene: O3 and H2O adsorption, benzo [a] pyrene degradation, and atmospheric implications, J. Phys. Chem. A, 105(16), 4029-4041, https://doi.org/10.1021/jp004137n, 2001.

Pye, H. O. T., Murphy, B. N., Xu, L., Ng, N. L., Carlton, A. G., Guo, H., Weber, R., Vasilakos, P., Appel, K. W., Budisulistiorini, S. H., Surratt, J. D., Nenes, A., Hu, W., Jimenez, J. L., Isaacman-VanWertz, G., Misztal, P. K., and Goldstein, A. H.: On the implications of aerosol liquid water and phase separation for organic aerosol mass, Atmos. Chem. Phys., 17, 343-369, https://doi.org/10.5194/acp-17-343-2017, 2017.

Radonić, J., Jovčić Gavanski, N., Ilić, M., Popov, S., Očovaj, S. B., Vojinović Miloradov, M., and Turk Sekulić, M.: Emission sources and health risk assessment of polycyclic aromatic hydrocarbons in ambient air during heating and non-heating periods in the city of Novi Sad, Serbia, Stoch. Environ. Res. Risk Assess., 31(9), 2201-2213, doi:10.1007/s00477-016-1372-x, 2017.

Rasool, Q. Z., Shrivastava, M., Octaviani, M., Zhao, B., Gaudet, B., and Liu, Y.: Modeling volatility-based aerosol phase state predictions in the Amazon rainforest, ACS Earth and Space Chem., 5, 10, 2910-2924, https://doi.org/10.1021/acsearthspacechem.1c00255, 2021.

Ringuet, J., Albinet, A., Leoz-Garziandia, E., Budzinski, H., and Villenave, E.: Reactivity of polycyclic aromatic compounds (PAHs, NPAHs and OPAHs) adsorbed on natural aerosol particles exposed to

971 atmospheric oxidants, Atmos. Environ., 61, 15-22, https://doi.org/10.1016/j.atmosenv.2012.07.025,
972 2012.

973 Saukko, E., Lambe, A. T., Massoli, P., Koop, T., Wright, J. P., Croasdale, D. R., Pedernera, D. A.,
974 Onasch, T. B., Laaksonen, A., Davidovits, P., Worsnop, D. R., and Virtanen, A.: Humidity-dependent
975 phase state of SOA particles from biogenic and anthropogenic precursors, Atmos. Chem. Phys., 12,
976 7517-7529, doi:10.5194/acp-12-7517-2012, 2012.

977 Schauer, C., Niessner, R., and Poschl, U.: Polycyclic aromatic hydrocarbons in urban air particulate
978 matter: decadal and seasonal trends, chemical degradation, and sampling artifacts, Environ. Sci. Technol.,
979 37(13), 2861-2868, https://doi.org/10.1021/es034059s, 2003.

980 Schmedding, R., Rasool, Q. Z., Zhang, Y., Pye, H. O. T., Zhang, H., Chen, Y., Surratt, J. D., Lopez-
981 Hilfiker, F. D., Thornton, J. A., Goldstein, A. H., and Vizuete, W.: Predicting secondary organic aerosol
982 phase state and viscosity and its effect on multiphase chemistry in a regional-scale air quality model,
983 Atmos. Chem. Phys., 20, 8201-8225, 10.5194/acp-20-8201-2020, 2020.

984 Sehili, A. M., and Lammel, G.: Global fate and distribution of polycyclic aromatic hydrocarbons emitted
985 from Europe and Russia, Atmos. Environ., 41(37), 8301-8315,
986 https://doi.org/10.1016/j.atmosenv.2007.06.050, 2007.

987 Shahpoury, P., Lammel, G., Albinet, A., Sofuoglu, A., Dumanoglu, Y., Sofuoglu, S. C., Wagner, Z., and
988 Zdimal, V.: Evaluation of a Conceptual Model for Gas-Particle Partitioning of Polycyclic Aromatic
989 Hydrocarbons Using Polyparameter Linear Free Energy Relationships, Environ. Sci. Technol., 50(22),
990 12312-12319, https://doi.org/10.1021/acs.est.6b02158, 2016.

991 Shen, H., Tao, S., Liu, J., Huang, Y., Chen, H., Li, W., Zhang, Y., Chen, Y., Su, S., Lin, N., Xu, Y., Li,
992 B., Wang, X., and Liu, W.: Global lung cancer risk from PAH exposure highly depends on emission
993 sources and individual susceptibility, Sci. Rep., 4, 6561, https://doi.org/10.1038/srep06561, 2014.

994 Shen, H., Huang, Y., Wang, R., Zhu, D., Li, W., Shen, G., Wang, B., Zhang, Y., Chen, Y., Lu, Y., Chen,
995 H., Li, T., Sun, K., Li, B., Liu, W., Liu, J., and Tao, S.: Global Atmospheric Emissions of Polycyclic
996 Aromatic Hydrocarbons from 1960 to 2008 and Future Predictions, Environ. Sci. Technol., 47(12), 6415-
997 6424, doi:10.1021/es400857z, 2013.

998 Srivastava, D., Tomaz, S., Favez, O., Lanzafame, G. M., Golly, B., Besombes, J.-L., Alleman, L. Y.,
999 Jaffrezo, J.-L., Jacob, V., Perraudin, E., Villenave, E. and Albinet, A.: Speciation of organic fraction
1000 does matter for source apportionment. Part 1: A one-year campaign in Grenoble (France), Sci. Total
1001 Environ., 624, 1598–1611, https://doi.org/10.1016/j.scitotenv.2017.12.135, 2018.

1002 Shiraiwa, M., Ammann, M., Koop, T., and Pöschl, U.: Gas uptake and chemical aging of s emisolid
1003 organic aerosol particles, Proc. Natl. Acad. Sci. U.S.A., 108(27), 11003-11008,
1004 https://doi.org/10.1073/pnas.1103045108, 2011.

1005 Shiraiwa, M., Li, Y., Tsimpidi, A. P., Karydis, V. A., Berkemeier, T., Pandis, S. N., Lelieveld, J., Koop,
1006 T., and Pöschl, U.: Global distribution of particle phase state in atmospheric secondary organic aerosols,
1007 Nat Commun, 8(1), 15002, https://doi.org/10.1038/ncomms15002, 2017.

1008 Shrivastava, M., Easter, R. C., Liu, X., Zelenyuk, A., Singh, B., Zhang, K., Ma, P.-L., Chand, D., Ghan,
1009 S., Jimenez, J. L., Zhang, Q., Fast, J., Rasch, P. J., and Tiitta, P.: Global transformation and fate of SOA:
1010 Implications of low-volatility SOA and gas-phase fragmentation reactions, J. Geophys. Res.: Atmos.,
1011 120(9), 4169-4195, https://doi.org/10.1002/2014JD022563, 2015.

Shrivastava, M., Lou, S., Zelenyuk, A., Easter, R. C., Corley, R. A., Thrall, B. D., Rasch, P. J., Fast, J. D., Massey Simonich, S. L., Shen, H., and Tao, S.: Global long-range transport and lung cancer risk from polycyclic aromatic hydrocarbons shielded by coatings of organic aerosol, Proc. Natl. Acad. Sci. U.S.A., 114(6), 1246-1251, https://doi.org/10.1073/pnas.1618475114, 2017.

Shrivastava, M., Rasool, Q. Z., Zhao, B., Octaviani, M., Zaveri, R. A., Zelenyuk, A., Gaudet, B., Liu, Y., Shilling, J. E., Schneider, J., Schulz, C., Zöger, M., Martin, S. T., Ye, J., Guenther, A., Souza, R. F., Wendisch, M., and Pöschl, U.: Tight Coupling of Surface and In-Plant Biochemistry and Convection Governs Key Fine Particulate Components over the Amazon Rainforest, ACS Earth and Space Chemistry, 6, 380-390, https://doi.org/10.1021/acsearthspacechem.1c00356, 2022.

Tomaz, S., P. Shahpoury, J. L. Jaffrezo, G. Lammel, E. Perraudin, E. Villenave, and A. Albinet: One-year study of polycyclic aromatic compounds at an urban site in Grenoble (France): Seasonal variations, gas/particle partitioning and cancer risk estimation, Sci Total Environ, 565, 1071-1083, https://doi.org/10.1016/j.scitotenv.2016.05.137, 2016.

Tørseth, K., Aas, W., Breivik, K., Fjæraa, A. M., Fiebig, M., Hjellbrekke, A.-G., Lund Myhre, C., Solberg, S., and Yttri, K. E.: Introduction to the European Monitoring and Evaluation Programme (EMEP) and observed atmospheric composition change during 1972–2009, Atmos. Chem. Phys., 12(12), 5447-5481, doi:10.5194/acp-12-5447-2012, 2012.

U.S. EPA. Carcinogen Assessment Of Coke Oven Emissions. U.S. Environmental Protection Agency, Washington, D.C., EPA/600/6-82/003F (NTIS PB84170182), 1982.

van der Werf, G. R., Randerson, J. T., Giglio, L., Collatz, G. J., Mu, M., Kasibhatla, P. S., Morton, D. C., DeFries, R. S., Jin, Y., and van Leeuwen, T. T.: Global fire emissions and the contribution of deforestation, savanna, forest, agricultural, and peat fires (1997-2009), Atmos. Chem. Phys., 10(23), 11707-11735, https://doi.org/10.5194/acp-10-11707-2010, 2010.

Van Overmeiren, P., Demeestere, K., Wispelaere, P. D., Gili, S., Mangold, A., Causmaecker, K. D., Mattielli, N., Delcloo, A., Langenhove, H. V., and Walgraeve, C.: Four years of active sampling and measurement of atmospheric polycyclic aromatic hydrocarbons and oxygenated polycyclic aromatic hydrocarbons in Dronning Maud Land, East Antarctica, Environ. Sci. Technol., 58, 1577-1588, https://doi.org/10.1021.acs.est.3c06425, 2024.

Wang, T., Xia, Z. H., Wu, M. M., Zhang, Q. Q., Sun, S. Q., Yin, J., Zhou, Y. C., and Yang, H.: Pollution characteristics, sources and lung cancer risk of atmospheric polycyclic aromatic hydrocarbons in a new urban district of Nanjing, China, J. Environ. Sci., 55, 118-128, https://doi.org/10.1016/j.jes.2016.06.025, 2017.

Wang, W., Simonich, S., Giri, B., Chang, Y., Chang, Y., Zhang, Y., Jia. Y., Tao, S., Wang, R., Wang, B., Li, W., Cao, J., and Lu, X.: Atmospheric concentrations and air-soil gas exchange of polycyclic aromatic hydrocarbons (PAHs) in remote, rural village and urban areas of Beijing-Tianjin region, North China, Sci. Total. Environ., 409(15), 2942-2950, https://doi.org/10.1016/j.scitotenv.2011.04.021, 2011.

Weber, S., Salameh, D., Albinet, A., Alleman, L. Y., Waked, A., Besombes, J.-L., Jacob, V., Guillaud, G., Meshbah, B., Rocq, B., Hulin, A., Dominik-Sègue, M., Chrétien, E., Jaffrezo, J.-L., and Favez, O.: Comparison of PM10 Sources Profiles at 15 French Sites Using a Harmonized Constrained Positive Matrix Factorization Approach, Atmos., 10, 310, https://doi.org/10.3390/atmos10060310, 2019.

WHO: Air quality guidelines for Europe, World Health Organization. Regional Office for Europe, 2000.

Wu, Z., Chen, X., Wang, Z., Chen, H., Wang, Z., Mu, Q., Wu, L., Wang, W., Tang, X., Li, J., Li, Y., Wu, Q., Wang, Y., Zou, Z., and Jiang, Z.: Modeling of polycyclic aromatic hydrocarbons (PAHs) from global to regional scales: model development (IAP-AACM_PAH v1.0) and investigation of health risks in 2013 and 2018 in China, Geosci. Model Dev., 17, 8885-8907, https://doi.org/10.5194/gmd-17-8885-2024, 2024.

Zelenyuk, A., Imre, D., Beranek, J., Abramson, E., Wilson, J., and Shrivastava, M.: Synergy between secondary organic aerosols and long-range transport of polycyclic aromatic hydrocarbons, Environ. Sci. Technol., 46(22), 12459-12466, https://doi.org/10.1021/es302743z, 2012.

Zhang, Y., Albinet, A., Petit, J.-E., Jacob, V., Chevrier, F., Gille, G., Pontet, S., Chrétien, E., Dominik-Sègue, M., Levigoureux, G., Močnik, G., Gros, V., Jaffrezo, J.-L., and Favez, O.: Substantial brown carbon emissions from wintertime residential wood burning over France, Sci. Total Environ., 743, 140752, https://doi.org/10.1016/j.scitotenv.2020.140752, 2020a.

Zhang, Y., Li, Z., Chen, Y., de Leeuw, G., Zhang, C., Xie, Y., and Li, K.: Improved inversion of aerosol components in the atmospheric column from remote sensing data, Atmos. Chem. Phys., 20(21), 12795-12811, https://doi.org/10.5194/acp-20-12795-2020, 2020b.

Zhang, Y., Nichman, L., Spencer, P., Jung, J. I., Lee, A., Heffernan, B. K., Gold, A., Zhang, Z., Chen, Y., Canagaratna, M. R., Jayne, J. T., Worsnop, D. R., Onasch, T. B., Surratt, J. D., Chandler, D., Davidovits, P., and Kolb, C. E.: The Cooling Rate and Volatility Dependent Glass Forming Properties of Organic Aerosols Measured by Broadband Dielectric Spectroscopy, Environ. Sci. Technol., https://doi.org/10.1021/acs.est.9b03317, 2019.

Zhang, Y. X., Tao, S., Shen, H. Z., and Ma, J. M.: Inhalation exposure to ambient polycyclic aromatic hydrocarbons and lung cancer risk of Chinese population, Proc. Natl. Acad. Sci. U.S.A., 106(50), 21063-21067, https://doi.org/10.1073/pnas.0905756106, 2009.

Zhou, S., Lee, A. K. Y., McWhinney, R. D., and Abbatt, J. P. D.: Burial Effects of Organic Coatings on the Heterogeneous Reactivity of Particle-Borne Benzo a pyrene (BaP) toward Ozone, J. Phys. Chem. A, 116(26), 7050-7056, https://doi.org/10.1021/jp3030705, 2012.

Zhou, S., Shiraiwa, M., McWhinney, R. D., Poschl, U., and Abbatt, J. P.: Kinetic limitations in gas-particle reactions arising from slow diffusion in secondary organic aerosol, Faraday Discuss, 165, 391-406, https://doi.org/10.1039/C3FD00030C, 2013.

Zhang, Z., Li, Y., Ran, H., An, J., Qu, Y., Zhou, W., Xu, W., Hu, W., Xie, H., Wang, Z., Sun, Y., and Shiraiwa, M.: Simulated phase state and viscosity of secondary organic aerosols over China, Atmos. Chem. Phys., 24, 4809-4826, https://doi.org/10.5194/acp-24-4809-2024, 2024.